Elastin-like Polypeptide-Based Bioink: A Promising Alternative for 3D Bioprinting.

Michèle Dai, Jean-Philippe Belaïdi, Guillaume Fleury, Elisabeth Garanger, Maïté Rielland, Xavier Schultze, Sébastien Lecommandoux

Author manuscript of article published in *Biomacromolecules*, DOI: 10.1021/acs.biomac.1c00861

Elastin-like polypeptide based bioink: a promising alternative for 3D bioprinting

Michèle Dai, [†,‡] *Jean-Philippe Belaïdi,* [†] *Guillaume Fleury,* [‡] *Elisabeth Garanger,* [‡] *Maïté Rielland,* [*,†] *Xavier Schultze,* [†] *Sébastien Lecommandoux*[‡]

[†] L'Oréal Recherche Avancée, 1 avenue Eugène Schueller, 93600, Aulnay-sous-Bois, France

[‡] Univ. Bordeaux, CNRS, Bordeaux INP, LCPO, UMR 5629, F-33600, Pessac, France

ABSTRACT:

Three-dimensional (3D) bioprinting offers a great alternative to traditional techniques in tissue reconstruction, based on seeding cells manually into scaffold, to better reproduce the organs complexity. When suitable bioink is engineered with appropriate physico-chemical properties, such process can advantageously provide a spatial control of the patterning that improve tissue reconstruction. The design of an adequate bioink must fulfill a long list of *criteria* including biocompatibility, printability and stability. In this context, we have developed a bioink containing a precisely controlled recombinant biopolymer, namely elastin-like polypeptide (ELP). This material was further chemo-selectively modified with cross-linkable moieties to provide a 3D network through photopolymerization. ELP chains were additionally either functionalized with a peptide sequence GRGDS (Gly-Arg-Gly-Asp-Ser) or combined with collagen I to enable cell-adhesion. Our ELP-based bioinks were found to be printable, while providing excellent

mechanical properties such as stiffness and elasticity in their cross-linked form. Besides, they were demonstrated to be biocompatible showing viability and adhesion of dermal normal human fibroblasts (NHF). Expressions of specific ECM protein markers as pro-collagen I, elastin, fibrillin and fibronectin were revealed within the 3D network containing cells after only 18 days of culture, showing the great potential of ELP-based bioinks for tissue engineering.

KEYWORDS. Recombinant elastin-like polypeptide, 3D bioprinting, Bioink, Tissue engineering

INTRODUCTION

Over the past decades, important progresses have been made in tissue engineering for regenerative medicine by providing tissue and organ substitutes to replace and restore damaged organ function [1–4]. This strategy can circumvent the limitations of current clinical treatments such as organ shortages which lead to patient's death before transplants are available [5,6]. The main approach involves seeding specific cells onto scaffolds attempting to lead to the function of the natural extracellular matrix and to provide a temporary support for the growth of target tissues. These tissue constructs can also replace animal models either for drug screening or disease modeling [7–9]. Conventional and mainly manual, approaches are moving on to advanced technologies to improve biomimetic structures. Among these techniques, three-dimensional (3D) bioprinting has emerged as one of the most promising tool to mimic the complexity of human organs while increasing the robustness of the reconstruction [10–12]. It allows an automated accurate deposition of cells, biomaterials and/or bioactive molecules forming the "bioink", to create a complex pre-programmed 3D tissue construct with good reproducibility [13,14]. The most challenging *criterion* for 3D bioprinting is to design a suitable bioink adapted to the specificities of both bioprinting technology and cells to print [15]. Shape fidelity, resolution but also biocompatibility and biofunctionnality complete the long list of desired properties in a bioink. Additionally, mechanical control is also extremely important either for printing process and for construct stability [16]. Among current biomaterials for bioinks composition, the most versatile ones are based on hydrogels, from which the 3D hydrated network can be used as a cell scaffold mimicking the extracellular matrix (ECM) [17–20]. Such architecture helps providing nutrients, oxygen and other required substrates, for the well-being of cells through their porosity [21].

In tissue engineering, researchers have used hydrogels with combination to proteins and carbohydrate-based materials such as collagen, fibrin, gelatin, hyaluronic acid, *etc* [22]. Indeed, their use provide bioinks with cell adhesion, proliferation and biological functionalities [19,23]. However, such bio-based materials generally suffer from batch-to-batch variations and low mechanical properties [12,24,25]. To overcome *in vivo* sourcing, biotechnological processes are being developed to produce both proteins and polysaccharides, allowing a better batch-to-batch reproducibility compared to bio-extracts. Though, the relatively high cost and the intrinsic difficulty to easily modify the structure of expressed proteins or polysaccharides are always detrimental for further applications. In this context, researchers have also explored synthetic hydrogels, to easily control the chemical design and thus, the physico-chemical properties [26]. Nevertheless, these hydrogels often lack biological ECM properties [21]. Therefore, a biomimetic ink combining the biological properties of bioinspired proteins or polysaccharides and the exquisite level of design achievable with synthetic polymers, could provide significant benefit for bioprinting and more generally tissue engineering.

Recombinant elastin-like polypeptides (ELPs) are considered as a very promising class of biocompatible protein-like polymers. They are composed of repeating sequences of -Val-Pro-Gly-*Xaa*-Gly- pentapeptides, where the guest residue *Xaa* can be any amino acid except proline [27,28]. They can be designed and produced with controlled sequences and molecular weight by recombinant DNA and protein engineering techniques. ELPs are derived from the hydrophobic domain of Tropoelastin, the precursor of Elastin, which is a key extracellular matrix protein that provides resilience and elasticity to many mammalian tissues, including skin, vasculature, elastic cartilage or lungs [27,29–31]. ELPs are promising candidates for tissue engineering as highlighted by several reports using ELP-based hydrogels [32–43]. In two recent studies, they were even used as an

ink component for tissue engineering through 3D bioprinting. Rodríguez-Cabello's team used a tetrablock of ELP combined with silk-like sequence for extrusion bioprinting [44]. They used one of the main properties of ELP which it its thermosensitivity [45] to fabricate their cell-loaded printed scaffold. Using amphiphilic ELP solutions at high concentration can lead to the formation of physical cross-linked hydrogels [46]. However, as several synthetic polymers, their ELP construct requires long time prior-dissolution (12 h) for proper use. As for Heilshorn's team, the scientists did not directly print ELPs with cells and their ink required a long-time process (5 to 30 minutes) to be cross-linked, which is of concern for cell viability and resolution of printing designs [47].

In the present study, we have selected an ELP, *MW*-ELP[V_3M_1-40], containing valine and methionine as guest residues, to fabricate an original and tunable bioink. Although recombinant DNA and protein engineering techniques are powerful methods to provide precision protein-based polymers, laborious molecular cloning steps can hamper the development of large libraries of ELPs. To avoid these steps, we have selectively modified methionine residues of our recombinant ELP by chemoselective post-modification reactions in order to confer new functionalities and properties [48,49]. We have in particular grafted acrylate moieties for chemical cross-linking through photopolymerization to form 3D networks, as well as the peptide sequence Gly-Arg-Gly-Asp-Ser (GRGDS) to allow cell adhesion. Indeed, GRGDS contains the amino acid sequence RGD which is a recognition site for the interactions between ECM macromolecules and cell membrane receptors [50]. We combined also our ELP with collagen I to enable cell-adhesion.

We have demonstrated that our different ELP-based bioinks are printable and can provide excellent mechanical properties such as stiffness and elasticity. They were shown to be biocompatible and enabled dermal normal human fibroblasts (NHF) adhesion and viability in presence of collagen or GRGDS peptide. The immunofluorescence studies of the 3D networks containing NHF showed

expressions of specific ECM protein dermal markers such as pro-collagen I, elastin, fibrillin and fibronectin. All those results show that ELP can be tailored to give specific ELP-based bioinks for 3D bioprinting in tissue engineering.

MATERIALS AND METHODS

Reagents and characterization techniques used were described in supporting information.

Recombinant MW-ELP[V_3M_1-40] synthesis

Recombinant *MW*-ELP[V_3M_1-40] was produced, isolated and purified according to previous studies [49]. The procedure was validated as described in supporting information *via* Figures S1-S4.

Chemoselective modification of MW-ELP[V_3M_1-40]

Synthesis of M(acrylate)W-ELP[V_3M(acrylate)$_1$-40]

MW-ELP[V_3M_1-40] was dissolved in an acetic acid/1,1,1,3,3,3-hexafluoro-2-propanol (HFIP) mixture (9/1 v/v) (20 mg/mL) and the solution was degassed by bubbling argon into the solution for 20 min. Glycidyl acrylate was added (10 equiv. per methionine residue) and the mixture was stirred for 48 hours under argon at 23°C. The solvents were evaporated under *vacuum* to give a viscous liquid. The latter was diluted with water and transferred to a 3 kDa Amicon centrifugal filter unit to be dialyzed against ultrapure water at 4°C. Then, the retentate was lyophilized to provide modified ELP as a white powder (yield > 50%). ^{1}H NMR (400.3 MHz, $CDCl_3$, 298K): δ 6.49 (dd, J = 17.2 Hz, 11H, -CH=CH_2), 6.24 (dd, J = 10.4 Hz, 11H, -CH=CH_2), 6.05 (dd, J = 10.4 Hz, 11H, -CH=CH_2), 4.64 (t, 11H, αCH_{Met}), 4.44 (m, 80H, 40 αCH_{Val} and 40 αCH_{Pro}), 4.17 (m, 30H, 30 αC$H_{Val\ as\ guest\ residue}$), 3.03 (s, 33H, -SC$H_3$), 1.92 (s, 33H, -C$H_3COO^-$). *To simplify the notation, M*(acrylate)*W*-ELP[V_3M(acrylate)$_1$-40] *is noted* ELPA in the following.

Synthesis of M(acrylate/30%GRGDS)W-ELP[V_3M(acrylate/30%GRGDS)$_1$-40]

ELPA (1 equiv.) and mercaptopropionic acid-(Gly-Arg-Gly-Asp-Ser)-OH (MPA-GRGDS-OH) (5 equiv. for 30 % targeted-GRGDS) were dissolved in ultrapure water. *N*-hexylamine (5 equiv.) was

added and the reaction mixture was stirred for 24 hours at 40°C. The solution was diluted with water and transferred to a 3 kDa Amicon centrifugal filter unit to be dialyzed against ultrapure water at 4°C. Then, the retentate was lyophilized to provide modified ELP as a white powder (yield > 50%). ^{1}H NMR (400.3 MHz, $CDCl_3$, 298K): δ 6.49 (dd, 7.7H, -CH=C*H*$_2$), 6.24 (dd, 7.7H, -C*H*=CH$_2$), 6.05 (dd, 7.7H, -CH=C*H*$_2$), 4.44 (m, 80H, αC*H*$_{Val}$ and αC*H*$_{Pro}$), 4.17 (m, 30H, αC*H*$_{Val\ as\ guest\ residue}$), 3.24 (t, *J* = 6.92 Hz, 6.6H, -NH-C*H*$_2$-CH$_2$- of Arg side chain), 3.03 (s, 33H, -SC*H*$_3$), 1.74-1.62 (br, 6.6H, -NH-CH$_2$-C*H*$_2$- of Arg side chain). *To simplify the notation, M*(acrylate/30%GRGDS)*W*-ELP[V$_3$M(acrylate/%GRGDS)$_1$-40] *is noted* ELPA-30%GRGDS in the following.

Cell culture

Dermal normal human fibroblasts (NHF) were obtained from patient's consent, from 18 years old Caucasian breast reduction surgery waste. For experiments, NHF present in cryopreserved vial were unthawed in a 37°C water bath, counted manually with a Bürker counting chamber (Blaubrand®), routinely cultured in fibroblast *medium* (FM) consisting of a DMEM (1X) + GlutaMAX supplemented with 10 % fetal bovine serum (Fe^{2+} supplemented) and 1 % antibiotic-antimycotic, and maintained in a humidified culture incubator at 37°C and with 5 % CO_2 until passage 7. They were cultured in T150 flask (Falcon) at an original density of 1 million cells to 13 million cells for 6 days in 25 mL of FM. *Medium* were changed every 2 days. When cells covered 70 to 90 % of the flask *area*, they were detached from the flask using 0.05 % Trypsin EDTA (1X) (Gibco) treatment for 3 minutes in a humidified culture incubator at 37°C and with 5 % CO_2. Treated cells were retrieved in FM and centrifuged at 1,000 rpm and used for specific purposes including viability, biocompatibility and reconstruction tests.

Bioinks formulation

All bioinks were made of 7.8 wt% of ELPA, dissolved in FM. For the sample containing GRGDS (named ELPA-GRGDS), 3.0 wt% of ELPA-30%GRGDS were added to the ELPA solution, while for the one with collagen I, (named ELPA-COLL), 0.13 wt% of collagen type I solution prepared on ice was added to the ELPA solution. 2 wt% of a stock solution at 6 wt% of CNF were then integrated to each solution. 0.025 wt% of lithium phenyl-2,4,6-trimethylbenzoylphosphinate (LAP) were weighted into each solution and the different sample vials were kept under aluminum foil. Solutions were mixed with a dual asymmetric centrifuge mixer (called also Speed Mixer) at 3,500 rpm during 3 minutes.

Bioink characterization

Printing pattern for rheology and swelling analysis

For these tests, the pattern generated through regenHU's BIOCAD software consists of three layers of a disk formed by a circle of 3.75 mm in radius filled with lines separated by 0.7 µm each. The printing process is described in 2.7.

Rheology measurement

Frequency sweep and creep experiments were conducted on an Anton Paar MCR-302 stress-controlled rheometer using the direct strain oscillation mode. The rheometer was outfitted with a Peltier heating system with an environmental trap for uniform temperature control. Hydrogels were loaded into an 8 mm sandblasted plate-and-plate geometry. A mineral oil barrier was used to prevent sample dehydration. Frequency sweeps were acquired from 0.1 to 100 rad/s at controlled temperatures with a strain amplitude of 0.1 %. Creep experiments were performed with an applied shear stress of 20 Pa and 200 Pa for 300 s followed by 500 s of recovery. The recovery can be

calculated *via* the equation: $\%R = \frac{(\gamma_c - \gamma_0) - (\gamma_r - \gamma_0)}{(\gamma_c - \gamma_0)} * 100$ where %R is the percent recovery, γ_0 the strain at the beginning of the creep period at 0 second, γ_c the strain at the end of the creep period at either 300 or 500 seconds and γ_r the strain at the end of the recovery period.

Swelling test

Three replicas of each bioink were printed in Petri dishes. Printed patterns were hydrated in 5 mL of FM for 10, 30, 60 minutes and 1, 2, 7 days of hydration for analysis. At each time point, FM were removed and excess around the hydrogel were eliminated with absorbent paper. Samples were then weighted w' and compared to non-hydrated initial bioink w_0 to determine the swelling ratio with the equation: swelling ratio (%) = $\frac{w'}{w_0} * 100$.

Bioprinting procedure

The formulated bioink was transferred into a 3cc cartridge and connected to a 300 µm diameter inkjet needle printhead (Needle CF-300 inner diameter (ID) = 0.3 mm, external diameter (ED) = 0.5 mm, length (L) = 2.4 mm (Ref. NCF-D0.3L2.41) containing a microvalve CF-300 nozzle diameter (ND) = 0.3 mm, stroke (S) = 0.1 mm (Ref. MVC-D0.3S0.1)), on a regenHU bioprinter. Prior to printing, a pattern was generated through regenHU's BIOCAD software. The pattern consists of two layers of a disk formed from a circle of 3.9 mm in radius filled with lines separated by 0.7 µm each, and two layers of an upper circle round the edge of the disk with 3.75 mm in radius. The design file was exported into a BIOCAD file format (.bcd) which was then imported into a file containing the G-code (.iso). This latter is readable by the HMI software which was able to list the instructions that control the movements and the tools of the regenHU bioprinter. The bioink was printed into a well-plate with a pressure set up at 0.030 MPa, a feed rate of 10 mm/s, a

dosing distance of 0.1 mm and a valve opening time of 2000 µs. While printed, the pattern was cross-linked under 15 seconds of 365 nm UV-light at 76.2 mW/cm².

Biocompatibility/viability tests

Prior to use live/dead kit and CellTiter-Glo® 3D kit for viability tests, samples were prepared and a circle of 600 µm in diameter of poly(ε-caprolactone)-ring were printed into each polycarbonate membrane insert (Skinsert, EpiSkin, #66.0053.302.611), placed in each well from 6-wells plates. 10 µl of bioink were added into PCL-rings. Each sample was exposed under UV-light at 365 nm for 15 seconds. 4 mL of FM were added, and plates were incubated either for 24 hours or 7 days in a humidified culture atmosphere at 37°C and with 5 % CO_2. In the case of 7 days, *media* were changed once, after 3 days. Then, live/dead kit was used for qualitative analysis. Briefly, samples *media* were removed and a solution containing calcein AM (0.125 µl/mL) and ethidium homodimer (0.5 µl/mL) was prepared in DPBS and was put in contact with samples for 30 minutes at room temperature in the dark Then, a Leica DMRB fluorescent microscope was used to visualize samples at x10 magnification. Samples were then recovered and used with CellTiter-Glo® 3D kit. Briefly, after 30 minutes of contact with the reagents provided by the kit, and transferred to a 96-well white plate (Corning), luminescent signals, more precisely relative light units (RLU) were measured with a GloMax® Discover Microplate Reader. Experiments were repeated four times for reproducibility.

Printed cell-laden scaffold

Construction process

Cell culture information, bioinks formulation and bioprinting procedure were defined in their respective sections, above. Briefly, prior to bioprinting, the dermal normal human fibroblast cells

at passage 7 were mixed in the bioink with the Speed Mixer at 1500 rpm during 30 seconds at a density of 2 million/mL. The suspension is then transferred into a 3cc cartridge (Nordson EFD) and placed onto the bioprinter. Scaffold containing fibroblast cells were printed through inkjet on a polycarbonate membrane and exposed under 365 nm UV-light at 76.2 mW/cm² during 15 s to immobilize the design. The printed pattern was immersed in FM. *Medium* was renewed every two days. At day 18, differentiated samples were collected and prepared for hematoxylin-eosin-saffron (HES) staining and immunohistochemistry analysis.

Fibroblast's functionality evaluation

After 18 days of culture, samples were collected and cut in half for analysis preparation. A part was protected by biopsy bag and placed in a histology cassette (Dutscher) which were then fixed in 4 % paraformaldehyde (w/v) buffered at pH 6.9 (Carlo Erba Reagents), for Haematoxylin-Eosin-Saffron (HES) staining. The other half is embedded in Tissue TEK (OCT compound #4583) in cryomold biopsy molds (Fisher) and frozen in a dry ice/100 % ethanol bath, for immunohistochemistry.

HES staining

Briefly, for the HES staining samples, they were dehydrated by a succession of ethanol 70 %, ethanol 100 % and xylene baths and were then inserted in paraffin. The samples were cut using a microtome at room temperature (RT) with a thickness of sections about 5 µm. Sections were placed into microscope slides (SuperFrost Plus, ThermoFischer) then rehydrated by xylene and decreased concentrations of ethanol. Sections were then immersed in hematoxylin solution for 2 minutes. They were washed and immersed in a bluing solution for 1 minute and washed again. They were then stained with 1 % eosin solution during 3 minutes. After the washing step, they were

dehydrated with ethanol and incubated in saffron for 2.5 minutes, rinsed in ethanol and xylene, and mounted with resin mounting *medium*. HES stained samples were achieved with a nanozoomer and analyzed with NanoZoomer Digital Pathology (NDP) view software.

Immunohistochemistry

Briefly, for the immunohistochemistry frozen samples, they were directly cut with a microtome connected to a cryostat at – 20°C with a thickness of sections about 7 µm. While cut, frozen sections were soaked 10 minutes in cold acetone at -20°C. Then, they were washed in PBS 1X for 10 minutes at room temperature. In the case of Vimentin, a permeabilization in PBS 1X/0.5 % Triton during 5 minutes at RT followed by a rinsing step in PBS 1X during 5 minutes at RT were performed. For all samples, non-specific sites were blocked in 3 % bovine serum albumin with 10 % normal goat serum during an hour at RT and incubated overnight with specific primary antibodies (See Table S1 for references). Then, the sections were rinsed 3 times with PBS 1X for 5 minutes at RT. AlexaFluor 555 conjugated secondary antibodies were added to the sections for 30 minutes to 1 hour depending on the sample at room temperature in dark chamber (See Table S1 for references). All sections were mounted using Prolong with DAPI. Immunofluorescence microscopy scans were achieved with a nanozoomer and analyzed with NDP view software.

RESULTS AND DISCUSSION

ELP-based bioink formulation

ELP functionalization by post-modification on its methionine residues

To fabricate a new and tunable bioink, an elastin-like polypeptide (ELP) was chosen as biopolymer backbone. More precisely, we obtained, using recombinant DNA and protein engineering techniques, *MW*-ELP[V_3M_1-40] which consists of 40 units of the pentapeptide -Val-Pro-Gly-*Xaa*-Gly- containing either methionine or valine residues at the *Xaa* positions (Figure S1). A methionine residue was incorporated every four ELP pentapeptide repeats for subsequent post-modifications and valine occupied the guest residue position in the other repeat units, leading to a Val:Met *ratio* of 3:1 at the guest residue position. At the *N*-terminus of the ELP, methionine and tryptophan (*MW*) residues were introduced (named "*Leader*") for proper initiation of the translation in *Escherichia coli* (*E. coli*) and ultra-violet/visible (UV/Vis) detection, respectively. The production, isolation and purification of this ELP are described in supplementary information (Figures S3-S4). *MW*-ELP[V_3M_1-40] is a perfectly defined biopolymer that can be tuned extensively by chemoselective post-modification of the 11 methionine residues, including one in the *Leader* sequence and 10 as guest residues in ELP pentapeptide repeats. At low pH, the thioether of methionine is the most nucleophilic group in proteins, over the *N*-terminal or lysine' side chain primary amines, histidine imidazoles as well as cysteine thiols, allowing them to chemoselectively react with various alkylating agents [51,52]. This technique can be used to introduce acrylate moieties on methionine residues which could then be cross-linked under UV light irradiation and in the presence of a photoinitiator. Glycidyl acrylate was therefore chosen for the addition to the thioether groups *via* an epoxide ring-opening reaction in acidic condition (Figure 1A).

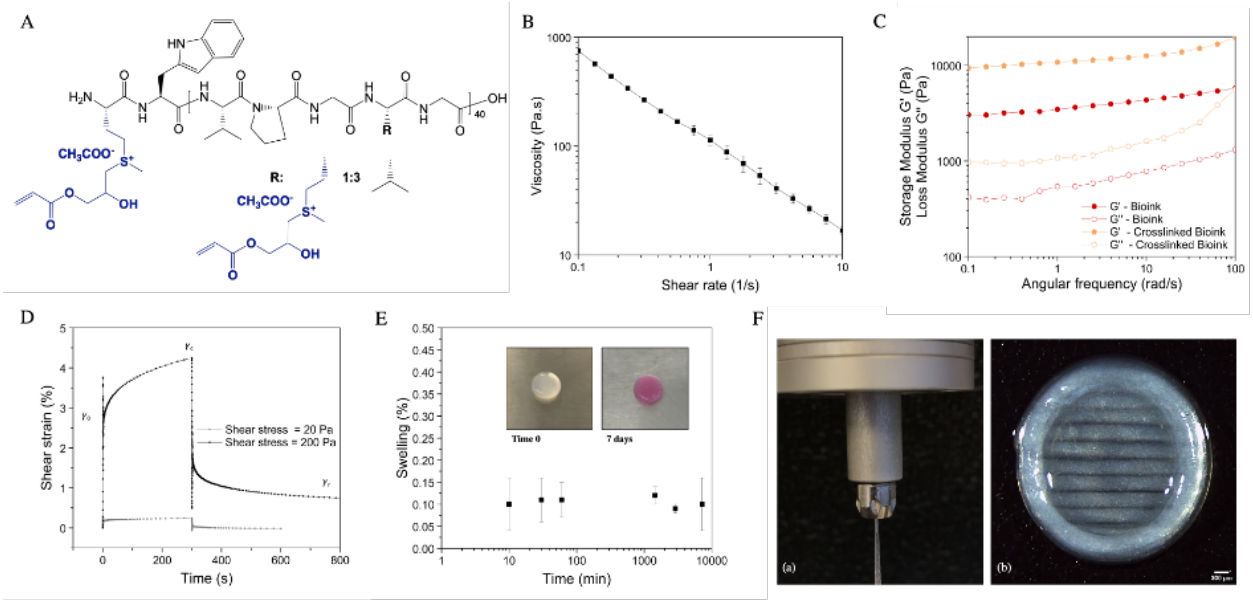

Figure 1. *ELPA used in a bioink.* **A** – Representation of acrylated *MW*-ELP[V_3M_1-40] elastin-like polypeptide. **B** – Rheological properties of uncross-linked ELPA-based bioink: viscosity η as function of shear rate $\dot{\gamma}$. **C** – Storage (G′, solid symbols) and loss (G″, open symbols) moduli as a function of angular frequency ω for a 0.1% strain amplitude at 22°C of cross-linked bioink compared to uncross-linked bioink. **D** – Viscoelastic results of creep tests on cross-linked bioink with shear stress τ = 20 and 200 Pa applied during 200 s followed by 300/500 s of relaxation, respectively. **E** – Swelling test on bioink in fibroblasts *medium* after 0, 10, 30, 60 minutes and 1, 2, 7 days of incubation at 37°C with 5%CO_2 with associated photographs of the bioink at time 0 and after 7 days. **F** - (a) Shear-thinning behavior of the ink. (b) Picture of the bioink-printed pattern, taken with a stereo microscope Leica M60 with an integrated Leica IC80 high-definition camera, scale bar: 300 μm.

The modified ELP (named thereafter ELPA), was then purified by solvent evaporation and dialysis against ultrapure water. The degree of functionalization (> 99 %) was assessed by ^{1}H NMR analysis (Figure S5). Acrylates are not only cross-linkable moieties but they can also react through thiol-Michael addition which is interesting for ELP functionalization [53]. By taking advantage of the GRGDS bioactive sequence, we performed a thiol-Michael addition reaction catalyzed by *N*-hexylamine in water using MPA-GRGDS-OH containing a thiol group at the *N*-terminal chain end of the peptide and ELPA. We selected 30% of GRGDS functionalization to preserve enough free acrylate motifs for the subsequent cross-linking process (named thereafter ELPA-GRGDS). The functionalized ELPs (ELPA and ELPA-GRGDS) were then purified by dialysis against ultrapure water and characterized by ^{1}H NMR (Figures S5, S6) showing the success of the modification.

Moreover, even if elastin-like polypeptides are known to be thermosensitive [54,55], including *MW*-(ELP[V_3M_1-40]), the methionine functionalization yielding ELPA and ELPA-30%GRGDS increased protein hydrophilicity as a consequence of the formation of the cationic sulfonium groups. Consequently, our modified ELPs do not show any thermoresponsiveness while used at concentration over 750 µM *i.e.,* over ~1.5% wt% for both ELP, in aqueous medium below 70°C, allowing a perfect solubility and ease of manipulation, as attested by dynamic light intensity (DLS) measurements (Figure S7).

Choice of a shear-thinning biomaterial and a photoinitiator

Non-cross-linked ELPA alone was too liquid to print a stable 3D design before reticulation but also to avoid sedimentation of cells during printing process. Thus, cellulose nanofibers (CNF) were chosen since, they can be 3D printed with specific mechanical properties, and they are biocompatible [56]. ELPA-based bioinks were thus formulated with a solution of cellulose nanofibers (CNF) at 2 wt% for printing, providing an adequate viscosity.

To cross-link our bioink after printing, we decided to use a LAP as photoinitiator. This compound has been used in hydrogel fabrication because of its water solubility and low toxicity in the range of efficiency [57–61]. Thus, we started to evaluate the range of LAP concentrations to obtain a gel with a sufficient macroscopic mechanical strength and stability. Results showed that a cross-linked hydrogel with sufficient stiffness and resistance through manipulation, can be obtained starting from 0.025 wt% of LAP and 15 seconds of 365 nm UV-exposure, with a minimum amount of 7.8 wt% ELPA (*data* not shown). Moreover, the potential cytotoxicity and phototoxicity of the LAP were evaluated on adult NHF. To do so, concentrations from 0 to 0.3 wt% of LAP, free in the culture media, were tested with or without UV light, and NHF morphology and survival were analysed after 24 hours (Figure S8). Results showed that without UV light exposure, LAP did not

have any cytotoxicity for all concentrations tested on NHF culture. However, UV-exposed LAP was cytotoxic above 0.025 wt%. To conclude, based on the first gelation trials and these cytotoxicity experiments, our ELPA bioink composition was fixed at 2 wt% CNF, 7.8 wt% ELPA and 0.025 wt% of LAP.

Printability of the bioink

To evaluate the printability of ELPA bioink, rheological properties were measured. The flow behavior was estimated at 22°C as printing would be performed at room temperature (Figure 1B). We observed that, in the range of applied shear rate (0.1 to 10 s^{-1}), the viscosity of the bioink decreased with increasing temperature according to a power law which illustrates the shear-thinning behavior of the ELPA bioinks (Figure 1B) often considered as a strong asset for 3D inkjet printing techniques. In addition, the storage and loss *moduli* (G' and G'', respectively) of the ELPA-based bioink were also determined in oscillatory shear using frequency sweep tests from 0.1 to 100 rad/s at specific temperatures: 10°C, 22°C and 40°C (Figure 1C red curves). Interestingly, a weak dependence of G' as well as a predominance of G' over G" (i.e. G'> G") were retrieved over the probed angular frequency range, highlighting a gel-like behavior.

Scaffold mechanical properties

An important *criterion* for bioink scaffolds is also to have mechanical feature close to the targeted tissue while providing ease of manipulation. Accordingly, the storage and loss *moduli* of the cross-linked ELP-based gel were measured under oscillatory shear at 22°C using a frequency sweep from 0.1 to 100 rad/s. A gel-like behavior was also retrieved over the probed range of angular frequency with characteristic G' values three times higher than the ones obtained for non-cross-linked bioink (Figure 1C orange curves). These results hinted the formation of an elastic network

formed by covalent cross-linking during the photopolymerization process. The high elasticity of our samples was also noticed when applying manual stresses. Indeed, as displayed in Figure S9 and Video S1, the recovery seemed to be complete after the removal of the stresses. To probe this behavior, we performed creep-recovery tests for a quantitative evaluation of ELPA elasticity. When a stress of 20 Pa was applied, the recovery was 100% while when 200 Pa was applied, the recovery was approximately 83 % after 500 s relaxation (Figure 1D). We further described the recovery process of the cross-linked bioinks by evaluating the strain recovery behavior after the creep tests as described in the supporting information (Figure S10, Table S2). Such analysis leads to the description of the recovery process through the characteristic relaxation time t_r which is related to the viscoelastic recovery process visualized after the instantaneous strain recovery. Relaxation times are of the same order of magnitude for both experiments performed (53.33 ± 4.91 s and 76.65 ± 2.20 s for an initial shear stress of 20 Pa and 200 Pa, respectively) and highlight the rapid recovery of the cross-linked bioinks under study. Moreover, no noticeable change in terms of macroscopic aspect of the sample, was visible after 7 days of incubation at 37°C with 5% CO_2 of the bioink in FM showing its stability over at least a week (Figure 1E photos). It is noteworthy that the red color of the hydrogel was due to the phenol red added in the culture medium, a pH indicator used in FM, revealing a homogeneous diffusion of the *medium* within the hydrogel. Thus, we also performed a swelling test by evaluating the amount of medium absorbed by the bioink over time, after 0 minute to 7 days (Figure 1E). The maximum swelling *ratio* did not exceed 8 % which was not significant. To summarize this part, our cross-linked bioink has a gel-like behavior, with limited swelling and is stable over a 7 day-culture period time.

Printing process

As the bioink exhibited shear-thinning property (Figure 1F(a)), inkjet bioprinting was chosen to construct scaffolds. Indeed, as reported, this technique offers a relatively high cell viability compared to extrusion bioprinting but needs shear-thinning materials [14,18]. The design of the scaffold included several layers of bioink containing dermal normal human fibroblast cells, and was constructed using a CAD software, as shown in the Figure 1F(b) and Video S2. More precisely, a 600 µm thickness patterned disk with an additional upper circle round the edge of the disk, was drawn, set up at a radius r = 3.9 mm, and printed to give an exploitable sample for further analyses, including hematoxylin-eosin-saffron (HES) staining and immunofluorescence (IF) experiments. As demonstrated by the Figure 1F(b) and Figure S11, the resolution given by inkjet bioprinting with the bioink was particularly compelling. To achieve this precision, different parameters were optimized to control the deposition including the pressure governing the flow speed set up at 0.030 MPa which is viable for cells. To avoid a drop-by-drop deposition and obtain a fiber-like deposition, we chose a nozzle diameter of 300 µm, a speed rate of the printing at 10 mm/s, a dosing distance of 0.1 mm and a valve opening time of 2000 µs which all contributed to an efficient and precise printing process. Printed pattern was then exposed under 365 nm UV-light at 76.2 mW/cm² during 15 s to cross-link the design structure. The printing was estimated at less than 1 minute per sample, which is an acceptable time for printing alive materials such as cells. To conclude, ELPA bioink was printable with good resolution.

Biocompatibility of the bioink

To analyze the biocompatibility of our bioink, we first performed experiments on manual deposition. Cell viability and attachment on ELPA alone and ELPA containing adhesion sites was evaluated using a live and dead kit based on fluorescence observation. To do so, we analyzed cell

viability and morphology after 24 hours and 7 days of NHF mixed with either ELPA alone, ELPA mixed with 0.13 wt% of collagen I bovine (ELPA-COLL) or 3 wt% of ELPA-30%GRGDS (ELPA-GRGDS) (Figure 2A).

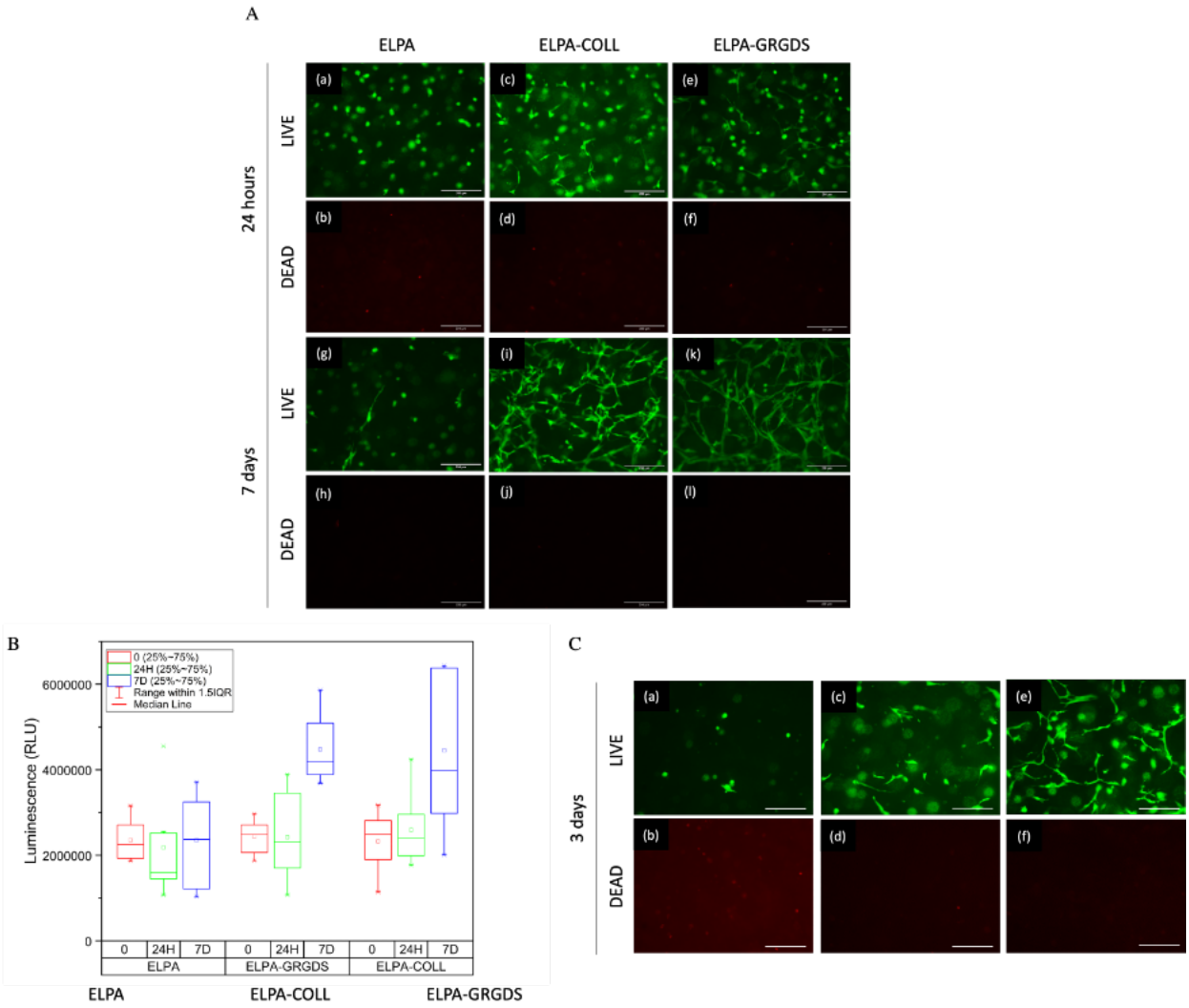

Figure. 2. Biocompatibility assays on 3D-cultured normal human fibroblast cells (NHF) in fibroblasts medium in ELP-based bioinks: ELPA, ELPA-COLL and ELPA-GRGDS. **A** – Live/dead test on NHF in ELP-based bioinks: (a, b – g, h) ELPA, (c, d – i, j) ELPA-COLL and (e, f – k, l) ELPA-GRGDS at 24 hours and 7 days, respectively scale bar = 200μm. **B** – Relative light units (RLU) via Cell-Titer Glo® 3D luminescent cell viability assay at T_0, after 24 hours and 7 days. **C** - Live/dead test on NHF in ELP-based bioinks: (a, b) ELPA, (c, d) ELPA-COLL and (e, f) ELPA-GRGDS, 3 days after printing, scale bar = 200 μm.

Results showed that in ELPA mix, NHF were still alive after 7 days (stained in green) but kept a round shape morphology showing that ELPA bioink did not allow NHF adhesion (Figure 2A(g)). In comparison, ELPA-COLL and ELPA-GRGDS enabled fibroblasts adhesion after 24 h as NHF

presented a characteristic dendritic morphology, associated with high cell survival at day 7 (Figures 2A(c, d, e, f, i, j, k, l)).

To confirm these results, quantitative measurements of ATP using CellTiterGlo® 3D kit were also achieved (Figure 2B). The *data* were interpreted and compared to live/dead tests results. Obtained luminescence data (RLU) are related to the ATP quantity and correlated to alive cells. Measurements were performed just after plating (time 0), 24 hours and 7 days after plating to follow cell viability.

In ELPA bioink, RLU *data* were non-significantly different between time 0, 24 hours and day 7 proving that cells remained alive and were metabolically active but did not proliferate. In ELPA-COLL and the ELPA-GRGDS bioinks, RLU were similar at time 0 and 24 hours. However, we observed a significant increase at day 7 for ELPA-GRGDS while it was difficult to observe the same phenomenon for ELPA-COLL due to larger *data* variability. To summarize, ELPA was biocompatible but did not allow NHF adhesion and proliferation. Adding an adhesion peptide to ELPA, either collagen I protein or GRGDS allowed NHF attachment and proliferation.

Finally, biocompatibility tests were performed after printing to validate that the printing process did not affect cell viability. To do so, ELPA, ELPA-COLL and ELPA-GRGDS were mixed with NHF, inkjet-printed, and then analyzed through live/dead test to evaluate the viability of the cells after 3 days (Figure 2C). Under stress, NHF within ELPA showed mainly dead cells (red fluorescence) with a small amount of viable round shaped cells (Figures 2C(a, b)). In this condition, as demonstrated above, cells did not adhere to the network. Thus, stress applied could be detrimental to cell viability. On the contrary, in ELPA-COLL and ELPA-GRGDS patterns, no dead cell were visible (Figures 2C(d, f)). To conclude, the printing process affected NHF viability in ELPA alone but had no impact on cell viability in ELPA-COLL and ELPA-GRGDS.

Cell functionality within the 3D bioprinted-networks

As ELPA, ELPA-COLL and ELPA-GRGDS bioinks, were printable and biocompatible we decided to evaluate the functionality of dermal human fibroblast within the bioprinted scaffolds. To do so, the different printed samples were submerged in FM and cultivated at 37°C in a humidified atmosphere containing 5 % of CO_2 for 18 days to let NHF settle down in the matrix and start producing extra-cellular matrix components.

To evaluate fibroblasts adhesion and organization within the 3D networks, samples were harvested at day 18 and analyzed by histological and immunofluorescence staining (Figures 3-4).

First, hematoxylin-eosin-saffron (HES) staining histology was performed allowing the visualization of the fibroblast's organization within the 3D networks, but also the structure of the reconstruction (Figure 3).

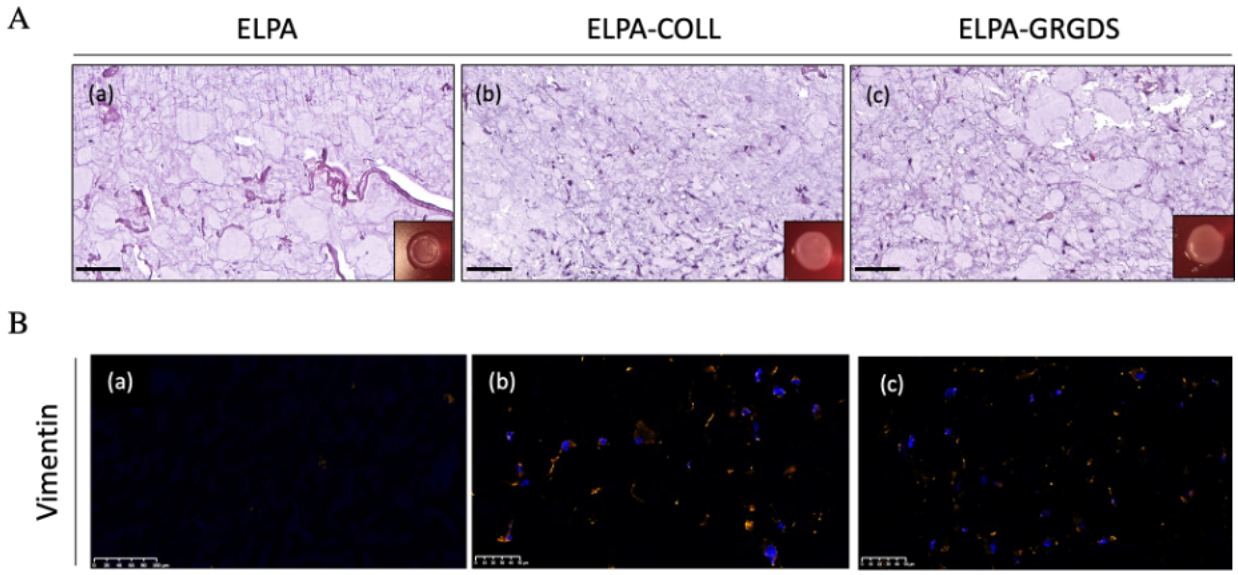

Figure 3. A – Hematoxylin-Eosin-Saffron (HES) staining histologies of (a) ELPA, (b) ELPA-COLL, (c) ELPA-GRGDS bioprinted 3D scaffolds with dermal normal human fibroblasts (NHF) in printed and their associated sample pictures (scale bar: 100 μm). **B** – Immunofluorescence staining on Vimentin of (a) ELPA, (b) ELPA-COLL, (c) ELPA-GRGDS, (X40, scale bar: 50 μm) proving the presence of dermal human fibroblasts in ELPA-COLL and ELPA-GRGDS but not in ELPA scaffold.

In ELPA samples, HES showed an absence of NHF (Figure 3A(a)) as expected. In the ELPA-COLL sample, fibroblasts can be found in the scaffold with a dendritic morphology proving that they have attached correctly. However, it was noticeable that many of them were close to the bottom of the construction, inducing a heterogeneity in the NHF repartition (Figure 3A(b)). In the case of ELPA-GRGDS, NHF was observed throughout the network, with a homogeneous distribution (Figure 3A(c)).

To confirm that the cells observed in ELPA-GRGDS and ELPA-COLL samples were NHF, we performed immunofluorescence (IF) on Vimentin, a fibroblast marker (Figure 3B). In the ELPA-COLL (Figure 3B(b)) and ELPA-GRGDS (Figure 3B(c)) networks, cells expressed Vimentin confirming that they were fibroblasts. In accordance with H&E staining, we did not find Vimentin expression in ELPA sample, (Figure 3B(a)).

We then decided to study the presence of extra-cellular matrix components (ECM) within the bioprinted scaffolds to assess functionality of NHF. Thus, expressions of Pro collagen I (1), collagen I (2), elastin (3), fibrillin (4) and fibronectin (5) were evaluated (Figure 4) in ELPA (a), ELPA-COLL (b) and ELPA-GRGDS (c) samples.

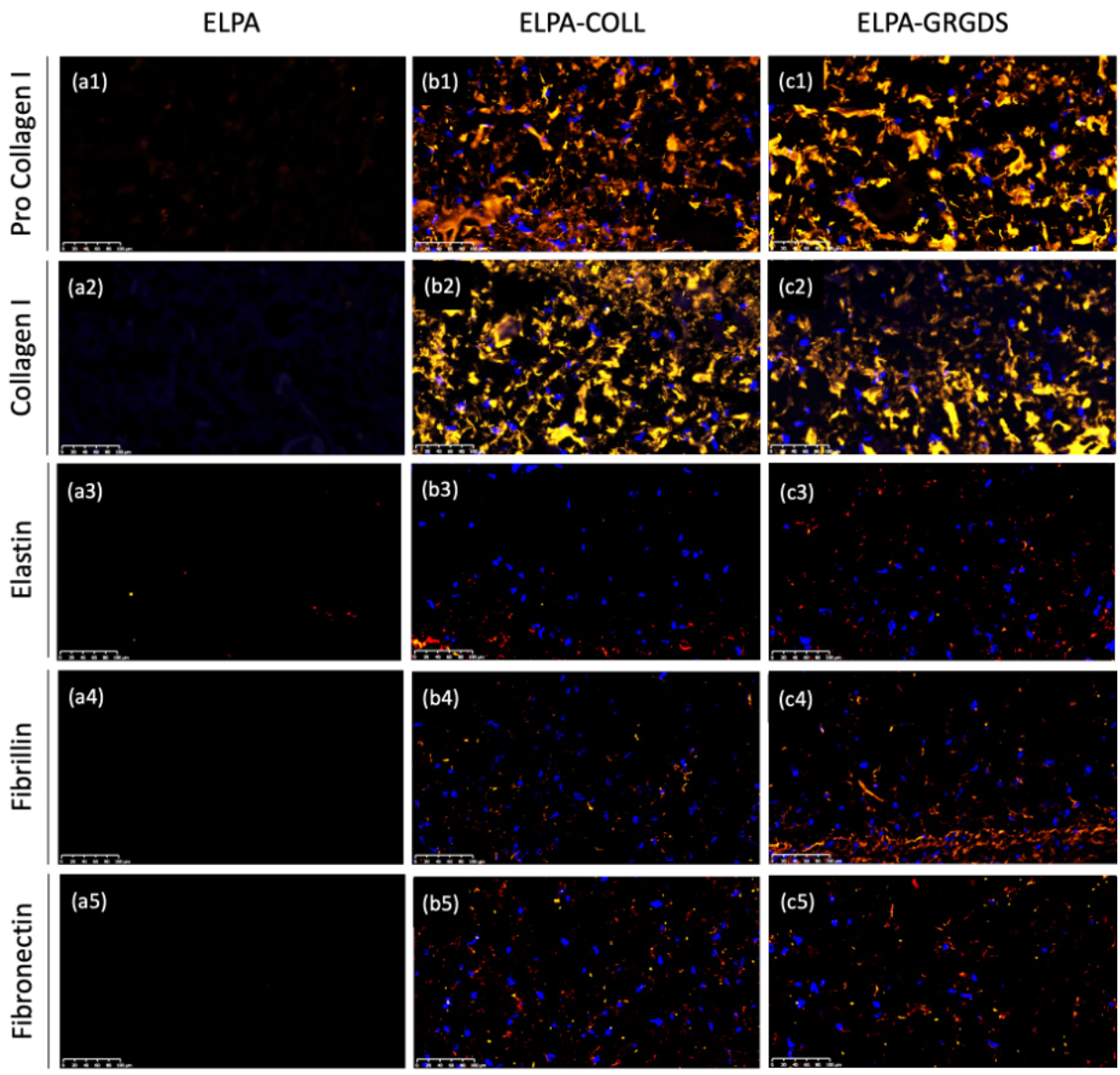

Figure 4. Immunofluorescence staining on (1) Pro collagen I, (2) collagen I, (3) elastin, (4) fibrillin, (5) fibronectin of ELP-based samples: (a) ELPA, (b) ELPA-COLL, (c) ELPA-GRGDS. (X20, Scale bar: 100 μm).

In ELPA samples, we could not observe any staining (Figures 4(a1-5)) which was consistent with our previous observation where no fibroblasts were present in the scaffold. In comparison, in ELPA-COLL (b) and ELPA-GRGDS (c) samples, Pro collagen I (1), collagen I (2), elastin (3), fibrillin (4) and fibronectin (5) were present which imply that fibroblasts have neo-synthetized extracellular matrix in these bioinks. Moreover, it seemed that Pro collagen I, fibrillin and elastin were more expressed in ELPA-GRGDS than in ELPA-COLL (b1, b3, b4 *vs.* c1, c3, c4

respectively) even if immunostaining is not a reliable quantitative method for proteins. These *data* showed that ELPA containing GRGDS is a great candidate as bioink but also as cell scaffold for tissue reconstruction.

Discussion

Since the early 2000s, 3D bioprinting procedures were developed and exploited extensively to improve the fabrication of human artificial tissues [62]. However, bioprinted constructs still lack of resemblance with human tissues [63]. This is often caused by the use of non-adapted bioink components. Indeed, it is important to choose a bioink which is compatible with bioprinting technology, and provide both suitable biological and mechanical properties [16].

In this study, we have formulated a bioink containing an Elastin-like polypeptide (ELP), *MW*-ELP[V_3M_1-40], produced with excellent purity and control over molecular weight and structure, since it was genetically encoded. Inspired from previous work in our laboratory on *MW*-ELP[V_3M_1-40] which has demonstrated the potential of modifying methionine residues through epoxide opening reaction to introduce specific functional moieties [49,64,65], we have generated acrylated ELP (ELPA) and ELPA-30%GRGDS. The introduction of acrylate groups on ELP allowed photo-cross linking, which was necessary to maintain printed patterns, while the introduction of GRGDS promoted cell adhesion. It also led to a stiff network that could enhance and promote fibroblasts proliferation [66] and could be an advantage in case of using rare cell types or to reduce the quantity of printed cells [67,68]. Furthermore, after chemical modification, ELPA and ELPA-GRGDS lost their thermosensitivity [49,54,55]. In a bioink formulation process, this became an advantage, as cells are sensitive to temperature [69] and the use of cooling/heating cartridges and/or temperature-controlled printing platform is not required. To be able to print liquid ELP bioinks with a good resolution, biocompatible cellulose nanofibers were introduced. This biomaterial

played a key role to provide adequate bioink consistency during printing and is probably responsible of the ELPA bioink shear-thinning behavior [56]. CNF has often been used in bioink compositions [56]. However, we are reporting for the first time, the use of CNF combined with ELP for bioink formulation. Moreover, ELPA bioink behaved as a gel-like structure, enabling a good support for cells before printing, as cells sediment when suspended in a liquid solution [70].

We also demonstrated the ability to provide a really good resolution of printed designs which can improve the quality of tissue constructs. After cross-linking, swelling tests showed that the 3D network remains stable over time (at least 7 days) which is a really interesting feature as many hydrogels could swell about a thousandfold their dry weight which is problematic to control the evolution of the tissue reconstruction [71]. The ink exhibits also an important ability to recover after applying a stress up to 200 Pa. This elasticity is close to human connective tissue environment and can play a role in ECM synthesis [72,73]. This could explain ECM protein neosynthesis by NHF in ELPA-GRGDS and ELPA-COLL after only 18 days of culture without any stimulation.

Biocompatibility studies of the bioink demonstrated that ELPA alone was not sufficient for cell adhesion. Indeed, cells stay round and do not spread into dendritic shape, a typical morphology of NHF within a 3D network [74]. If NHF cannot attach they die in couple of days [75]. This is exactly what we observe in ELPA scaffold after 18 days of culture where no remaining cells were present, probably evacuated with media changes during culture period. Thus, collagen I was introduced, contributing to cell adhesion through its cell-binding domains [76]. Collagen I is a commonly used biomaterial for organ reconstruction as it is the main protein present in the connective tissues [77]. However, the animal origin of our collagen I imply batch-to-batch variations. Moreover, collagen is also difficult to handle due to its sensitive gelation process and its tendency to contract in the presence of fibroblasts [78] over time can change pattern shape [79]. In comparison, using ELPA-

30%GRGDS provides a better cell adhesion, with a typical dendritic morphology of the fibroblasts after 3 days, which would suggest that the kinetic of attachment is faster in ELPA-GRGDS than in ELPA-COLL and could be a great alternative to collagen. Compared to several contributions that focus only on fibroblast viability within printed pattern [80–83], we have demonstrated here that our network is suitable for fibroblasts viability but also for correct adhesion, an important point for further cell differentiation and proliferation [84].

In addition, ELPA containing cell adhesion sites enables dermal normal fibroblast to recover a secretory behavior *in vitro*. We have actually found that NHF in ELPA-GRGDS and ELPA-COLL were neosynthetizing specific proteins of the dermal ECM as Pro collagen I, elastin, fibrillin or fibronectin [85]. It is really interesting to find elastin expression as it is relatively rare in skin substitute [86]. It is even more rare with the use of a bioink for skin tissue engineering [87–95]. Thus, our bioink has great potential for skin reconstruction especially skin bioprinting. Based on those promising results, it would be interesting to optimize printing conditions to skin bioprinting with a dermal-like scaffold with NHF and keratinocytes seeded or printed on top of it.

CONCLUSION

We developed a unique, easily and precisely tunable ELP and demonstrated a real potential of bioinks using ELP containing cell adhesive motifs for tissue substitutes. Our ELP-based bioink has demonstrated excellent mechanical properties such as stiffness and elasticity but also when combined with GRGDS or collagen, biological properties such as fibroblasts viability, adhesion and ECM neosynthesis. These parameters enabled 3D bioprinting easily a physiological network with good resolution, As ELP is a controllable and versatile biopolymer, it could be extensively

tuned to provide desired properties and thus, to make ideal bioink for various specific purposes in regenerative medicine especially in skin reconstruction.

ASSOCIATED CONTENT

Supporting Information

The supporting information including: a/ Reagents, b/ Characterization techniques, c/ Development and characterization of MW-ELP[V_3M_1-40], d/ Characterization of modified MW-ELP[V_3M_1-40] with acrylates, e/ Characterization of modified MW-ELP[V_3M_1-40] with GRGDS, f/ Loss of thermosensitivity through post-modification of ELP, g/ Evaluation of LAP toxicity and phototoxicity, h/ Bioink elasticity (Video S1) and i/ Printing fidelity (Video S2) is available free of charge on the ACS Publications website at DOI:

AUTHOR INFORMATION

Corresponding Author

* *Correspondence to maite.rielland@rd.loreal.com.*

Author Contributions

MD: performed all experiments, methodology, writing original draft preparation

JPB: co-performed bioprinting biological and Tissue engineering experiments, methodology

GF: co-performed rheological experiments

EG: co-performed bio-productions and chemical characterization

MR: project administration of the biological and Tissue Engineering part, supervision for the biological and Tissue Engineering part, reviewing and editing original draft

XS and SL: PhD directors, supervision, funding acquisition, project administration of the chemical part, reviewing and editing original draft

Funding sources

This work was supported by CIFRE grant from ANRT.

Notes

The authors declare that they have no competing interests.

ACKNOWLEDGEMENTS

The authors would also like to acknowledge Virginie Flouret for her advice in reconstruction, Stéphanie Desbouis for her advice in microscopy, Marion Plessis and Franck Hernandez for their help in the laboratory and Atlantic Bones Screen (ABS) in Saint Herblain for the HES and IF analysis.

REFERENCES

(1) Ikada, Y. Challenges in Tissue Engineering. *J. R. Soc. Interface* **2006**, *3* (10), 589–601. https://doi.org/10.1098/rsif.2006.0124.

(2) Atala, A. Engineering Organs. *Curr. Opin. Biotechnol.* **2009**, *20* (5), 575–592. https://doi.org/https://doi.org/10.1016/j.copbio.2009.10.003.

(3) Dzobo, K.; Thomford, N. E.; Senthebane, D. A.; Shipanga, H.; Rowe, A.; Dandara, C.; Pillay, M.; Motaung, K. S. C. M. Advances in Regenerative Medicine and Tissue Engineering: Innovation and Transformation of Medicine. *Stem Cells Int.* **2018**, *2018*, 2495848. https://doi.org/10.1155/2018/2495848.

(4) Ramos, T.; Moroni, L. Tissue Engineering and Regenerative Medicine 2019: The Role of Biofabrication—A Year in Review. *Tissue Eng. Part C Methods* **2019**, *26* (2), 91–106. https://doi.org/10.1089/ten.tec.2019.0344.

(5) Hunsberger, J.; Neubert, J.; Wertheim, J. A.; Allickson, J.; Atala, A. Bioengineering Priorities on a Path to Ending Organ Shortage. *Curr. Stem Cell Reports* **2016**, *2* (2), 118–127. https://doi.org/10.1007/s40778-016-0038-4.

(6) Heidary Rouchi, A.; Mahdavi-Mazdeh, M. Regenerative Medicine in Organ and Tissue Transplantation: Shortly and Practically Achievable? *Int. J. organ Transplant. Med.* **2015**, *6* (3), 93–98.

(7) Nam, K.-H.; Smith, A. S. T.; Lone, S.; Kwon, S.; Kim, D.-H. Biomimetic 3D Tissue Models for Advanced High-Throughput Drug Screening. *J. Lab. Autom.* **2015**, *20* (3), 201–215. https://doi.org/10.1177/2211068214557813.

(8) Tissue-Engineered Disease Models. *Nat. Biomed. Eng.* **2018**, *2* (12), 879–880. https://doi.org/10.1038/s41551-018-0339-2.

(9) Bédard, P.; Gauvin, S.; Ferland, K.; Caneparo, C.; Pellerin, È.; Chabaud, S.; Bolduc, S. Innovative Human Three-Dimensional Tissue-Engineered Models as an Alternative to Animal Testing. *Bioeng. (Basel, Switzerland)* **2020**, *7* (3), 115. https://doi.org/10.3390/bioengineering7030115.

(10) Matai, I.; Kaur, G.; Seyedsalehi, A.; McClinton, A.; Laurencin, C. T. Progress in 3D Bioprinting Technology for Tissue/Organ Regenerative Engineering. *Biomaterials* **2020**, *226*, 119536. https://doi.org/https://doi.org/10.1016/j.biomaterials.2019.119536.

(11) Agarwal, S.; Saha, S.; Balla, V. K.; Pal, A.; Barui, A.; Bodhak, S. Current Developments in 3D Bioprinting for Tissue and Organ Regeneration–A Review. *Front. Mech. Eng.* **2020**, *6*, 90.

(12) Ahadian, S.; Khademhosseini, A. A Perspective on 3D Bioprinting in Tissue Regeneration. *Bio-design Manuf.* **2018**, *1* (3), 157–160. https://doi.org/10.1007/s42242-018-0020-3.

(13) Wlodarczyk-Biegun, M.; del Campo, A. 3D Bioprinting of Structural Proteins. *Biomaterials* **2017**, *134*, 180–201. https://doi.org/10.1016/j.biomaterials.2017.04.019.

(14) Murphy, S. V; Atala, A. 3D Bioprinting of Tissues and Organs. *Nat. Biotechnol.* **2014**, *32*, 773.

(15) Theus, A.S.; Ning, L.; Hwang, B.; Gil, C.; Chen, S.; Wombwell, A.; Mehta, R.; Serpooshan, V. Bioprintability: Physiomechanical and Biological Requirements of Materials for 3D Bioprinting Processes. *Polymers (Basel).* **2020**, *12*, 2262.

(16) Chimene, D.; Lennox, K. K.; Kaunas, R. R.; Gaharwar, A. K. Advanced Bioinks for 3D Printing: A Materials Science Perspective. *Ann. Biomed. Eng.* **2016**, *44* (6), 2090–2102. https://doi.org/10.1007/s10439-016-1638-y.

(17) Tibbitt, M. W.; Anseth, K. S. Hydrogels as Extracellular Matrix Mimics for 3D Cell Culture.

Biotechnol. Bioeng. **2009**, *103* (4), 655–663. https://doi.org/10.1002/bit.22361.

(18) Valot, L.; Martinez, J.; Mehdi, A.; Subra, G. Chemical Insights into Bioinks for 3D Printing. *Chem. Soc. Rev.* **2019**, *48*, 4049–4086. https://doi.org/10.1039/C7CS00718C.

(19) Gopinathan, J.; Noh, I. Recent Trends in Bioinks for 3D Printing. *Biomater. Res.* **2018**, *22*, 11. https://doi.org/10.1186/s40824-018-0122-1.

(20) Gungor-Ozkerim, P. S.; Inci, I.; Zhang, Y. S.; Khademhosseini, A.; Dokmeci, M. R. Bioinks for 3D Bioprinting: An Overview. *Biomater. Sci.* **2018**, *6* (5), 915–946. https://doi.org/10.1039/c7bm00765e.

(21) Spicer, C. D. Hydrogel Scaffolds for Tissue Engineering: The Importance of Polymer Choice. *Polym. Chem.* **2020**, *11* (2), 184–219. https://doi.org/10.1039/C9PY01021A.

(22) Brovold, M.; Almeida, J. I.; Pla-Palacín, I.; Sainz-Arnal, P.; Sánchez-Romero, N.; Rivas, J. J.; Almeida, H.; Dachary, P. R.; Serrano-Aulló, T.; Soker, S.; Baptista, P. M. Naturally-Derived Biomaterials for Tissue Engineering Applications. *Adv. Exp. Med. Biol.* **2018**, *1077*, 421–449. https://doi.org/10.1007/978-981-13-0947-2_23.

(23) Kanta, J. Collagen Matrix as a Tool in Studying Fibroblastic Cell Behavior. *Cell Adh. Migr.* **2015**, *9* (4), 308–316. https://doi.org/10.1080/19336918.2015.1005469.

(24) Nicholas, M. N.; Jeschke, M. G.; Amini-Nik, S. Methodologies in Creating Skin Substitutes. *Cell. Mol. Life Sci.* **2016**, *73* (18), 3453–3472. https://doi.org/10.1007/s00018-016-2252-8.

(25) Gasperini, L.; Mano, J. F.; Reis, R. L. Natural Polymers for the Microencapsulation of Cells. *J. R. Soc. Interface* **2014**, *11* (100), 20140817. https://doi.org/10.1098/rsif.2014.0817.

(26) Jeong, K.-H.; Park, D.; Lee, Y.-C. Polymer-Based Hydrogel Scaffolds for Skin Tissue Engineering Applications: A Mini-Review. *J. Polym. Res.* **2017**, *24* (7), 112. https://doi.org/10.1007/s10965-017-1278-4.

(27) Wise, S. G.; Weiss, A. S. Tropoelastin. *Int. J. Biochem. Cell Biol.* **2009**, *41* (3), 494–497. https://doi.org/https://doi.org/10.1016/j.biocel.2008.03.017.

(28) Roberts, S.; Dzuricky, M.; Chilkoti, A. Elastin-like Polypeptides as Models of Intrinsically Disordered Proteins. *FEBS Lett.* **2015**, *589* (19, Part A), 2477–2486. https://doi.org/https://doi.org/10.1016/j.febslet.2015.08.029.

(29) Daamen, W. F.; Veerkamp, J. H.; van Hest, J. C. M.; van Kuppevelt, T. H. Elastin as a Biomaterial for Tissue Engineering. *Biomaterials* **2007**, *28* (30), 4378–4398. https://doi.org/https://doi.org/10.1016/j.biomaterials.2007.06.025.

(30) Yeo, G. C.; Aghaei-Ghareh-Bolagh, B.; Brackenreg, E. P.; Hiob, M. A.; Lee, P.; Weiss, A. S. Fabricated Elastin. *Adv. Healthc. Mater.* **2015**, *4* (16), 2530–2556. https://doi.org/10.1002/adhm.201400781.

(31) Stojic, M.; Ródenas-Rochina, J.; López-Donaire, M. L.; González de Torre, I.; González Pérez, M.; Rodríguez-Cabello, J. C. Elastin-Plasma Hybrid Hydrogels for Skin Tissue

Engineering. *Polymers (Basel).* **2021**, *13* (13), 2114.

(32) Nettles, D. L.; Chilkoti, A.; Setton, L. A. Applications of Elastin-like Polypeptides in Tissue Engineering. *Adv. Drug Deliv. Rev.* **2010**, *62* (15), 1479–1485. https://doi.org/10.1016/j.addr.2010.04.002.

(33) Betre, H.; Setton, L. A.; Meyer, D. E.; Chilkoti, A. Characterization of a Genetically Engineered Elastin-like Polypeptide for Cartilaginous Tissue Repair. *Biomacromolecules* **2002**, *3* (5), 910–916. https://doi.org/10.1021/bm0255037.

(34) Meco, E.; Lampe, K. J. Impact of Elastin-like Protein Temperature Transition on PEG-ELP Hybrid Hydrogel Properties. *Biomacromolecules* **2019**, *20* (5), 1914–1925. https://doi.org/10.1021/acs.biomac.9b00113.

(35) Shmidov, Y.; Zhou, M.; Yosefi, G.; Bitton, R.; Matson, J. B. Hydrogels Composed of Hyaluronic Acid and Dendritic ELPs: Hierarchical Structure and Physical Properties. *Soft Matter* **2019**, *15* (5), 917–925. https://doi.org/10.1039/C8SM02450B.

(36) McHale, M. K.; Setton, L. A.; Chilkoti, A. Synthesis and in Vitro Evaluation of Enzymatically Cross-Linked Elastin-Like Polypeptide Gels for Cartilaginous Tissue Repair. *Tissue Eng.* **2005**, *11* (11–12), 1768–1779. https://doi.org/10.1089/ten.2005.11.1768.

(37) Annabi, N.; Mithieux, S. M.; Boughton, E. A.; Ruys, A. J.; Weiss, A. S.; Dehghani, F. Synthesis of Highly Porous Crosslinked Elastin Hydrogels and Their Interaction with Fibroblasts in Vitro. *Biomaterials* **2009**, *30* (27), 4550–4557. https://doi.org/https://doi.org/10.1016/j.biomaterials.2009.05.014.

(38) Nagapudi, K.; Brinkman, W. T.; Leisen, J. E.; Huang, L.; McMillan, R. A.; Apkarian, R. P.; Conticello, V. P.; Chaikof, E. L. Photomediated Solid-State Cross-Linking of an Elastin−Mimetic Recombinant Protein Polymer. *Macromolecules* **2002**, *35* (5), 1730–1737. https://doi.org/10.1021/ma011429t.

(39) Trabbic-Carlson, K.; Setton, L. A.; Chilkoti, A. Swelling and Mechanical Behaviors of Chemically Cross-Linked Hydrogels of Elastin-like Polypeptides. *Biomacromolecules* **2003**, *4* (3), 572–580. https://doi.org/10.1021/bm025671z.

(40) Mithieux, S. M.; Rasko, J. E. J.; Weiss, A. S. Synthetic Elastin Hydrogels Derived from Massive Elastic Assemblies of Self-Organized Human Protein Monomers. *Biomaterials* **2004**, *25* (20), 4921–4927. https://doi.org/https://doi.org/10.1016/j.biomaterials.2004.01.055.

(41) Wang, H.; Cai, L.; Paul, A.; Enejder, A.; Heilshorn, S. C. Hybrid Elastin-like Polypeptide–Polyethylene Glycol (ELP-PEG) Hydrogels with Improved Transparency and Independent Control of Matrix Mechanics and Cell Ligand Density. *Biomacromolecules* **2014**, *15* (9), 3421–3428. https://doi.org/10.1021/bm500969d.

(42) Gonzalez, M. A.; Simon, J. R.; Ghoorchian, A.; Scholl, Z.; Lin, S.; Rubinstein, M.; Marszalek, P.; Chilkoti, A.; López, G. P.; Zhao, X. Strong, Tough, Stretchable, and Self-

Adhesive Hydrogels from Intrinsically Unstructured Proteins. *Adv. Mater.* **2017**, *29* (10), 1604743. https://doi.org/10.1002/adma.201604743.

(43) Shirzaei Sani, E.; Portillo-Lara, R.; Spencer, A.; Yu, W.; Geilich, B. M.; Noshadi, I.; Webster, T. J.; Annabi, N. Engineering Adhesive and Antimicrobial Hyaluronic Acid/Elastin-like Polypeptide Hybrid Hydrogels for Tissue Engineering Applications. *ACS Biomater. Sci. Eng.* **2018**, *4* (7), 2528–2540. https://doi.org/10.1021/acsbiomaterials.8b00408.

(44) Salinas-Fernández, S.; Santos, M.; Alonso, M.; Quintanilla, L.; Rodríguez-Cabello, J. C. Genetically Engineered Elastin-like Recombinamers with Sequence-Based Molecular Stabilization as Advanced Bioinks for 3D Bioprinting. *Appl. Mater. Today* **2020**, *18*, 100500. https://doi.org/https://doi.org/10.1016/j.apmt.2019.100500.

(45) Meyer, D. E.; Chilkoti, A. Purification of Recombinant Proteins by Fusion with Thermally-Responsive Polypeptides. *Nat. Biotechnol.* **1999**, *17* (11), 1112–1115. https://doi.org/10.1038/15100.

(46) Dai, M.; Goudounet, G.; Zhao, H.; Garbay, B.; Garanger, E.; Pecastaings, G.; Schultze, X.; Lecommandoux, S. Thermosensitive Hybrid Elastin-like Polypeptide-Based ABC Triblock Hydrogel. *Macromolecules* **2021**, *54* (1), 327–340. https://doi.org/10.1021/acs.macromol.0c01744.

(47) Duarte Campos, D. F.; Lindsay, C. D.; Roth, J. G.; LeSavage, B. L.; Seymour, A. J.; Krajina, B. A.; Ribeiro, R.; Costa, P. F.; Blaeser, A.; Heilshorn, S. C. Bioprinting Cell- and Spheroid-Laden Protein-Engineered Hydrogels as Tissue-on-Chip Platforms . *Frontiers in Bioengineering and Biotechnology* . 2020, p 374.

(48) Kramer, J. R.; Petitdemange, R.; Bataille, L.; Bathany, K.; Wirotius, A.-L.; Garbay, B.; Deming, T. J.; Garanger, E.; Lecommandoux, S. Quantitative Side-Chain Modifications of Methionine-Containing Elastin-Like Polypeptides as a Versatile Tool to Tune Their Properties. *ACS Macro Lett.* **2015**, *4* (11), 1283–1286. https://doi.org/10.1021/acsmacrolett.5b00651.

(49) Petitdemange, R.; Garanger, E.; Bataille, L.; Bathany, K.; Garbay, B.; Deming, T. J.; Lecommandoux, S. Tuning Thermoresponsive Properties of Cationic Elastin-like Polypeptides by Varying Counterions and Side-Chains. *Bioconjug. Chem.* **2017**, *28* (5), 1403–1412. https://doi.org/10.1021/acs.bioconjchem.7b00082.

(50) Bellis, S. L. Advantages of RGD Peptides for Directing Cell Association with Biomaterials. *Biomaterials* **2011**, *32* (18), 4205–4210. https://doi.org/10.1016/j.biomaterials.2011.02.029.

(51) Gharakhanian, E. G.; Deming, T. J. Chemoselective Synthesis of Functional Homocysteine Residues in Polypeptides and Peptides. *Chem. Commun.* **2016**, *52* (30), 5336–5339. https://doi.org/10.1039/C6CC01253A.

(52) Deming, T. J. Functional Modification of Thioether Groups in Peptides, Polypeptides, and Proteins. *Bioconjug. Chem.* **2017**, *28* (3), 691–700.

https://doi.org/10.1021/acs.bioconjchem.6b00696.

(53) Li, G.-Z.; Randev, R. K.; Soeriyadi, A. H.; Rees, G.; Boyer, C.; Tong, Z.; Davis, T. P.; Becer, C. R.; Haddleton, D. M. Investigation into Thiol-(Meth)Acrylate Michael Addition Reactions Using Amine and Phosphine Catalysts. *Polym. Chem.* **2010**, *1* (8), 1196–1204. https://doi.org/10.1039/C0PY00100G.

(54) Urry, D. W.; Long, M. M.; Cox, B. A.; Ohnishi, T.; Mitchell, L. W.; Jacobs, M. The Synthetic Polypentapeptide of Elastin Coacervates and Forms Filamentous Aggregates. *Biochim. Biophys. Acta - Protein Struct.* **1974**, *371* (2), 597–602. https://doi.org/https://doi.org/10.1016/0005-2795(74)90057-9.

(55) Urry, D. W.; Gowda, D. C.; Parker, T. M.; Luan, C.-H.; Reid, M. C.; Harris, C. M.; Pattanaik, A.; Harris, R. D. Hydrophobicity Scale for Proteins Based on Inverse Temperature Transitions. *Biopolymers* **1992**, *32* (9), 1243–1250. https://doi.org/10.1002/bip.360320913.

(56) Athukoralalage, S. S.; Balu, R.; Dutta, N. K.; Roy Choudhury, N. 3D Bioprinted Nanocellulose-Based Hydrogels for Tissue Engineering Applications: A Brief Review. *Polymers (Basel).* **2019**, *11* (5), 898. https://doi.org/10.3390/polym11050898.

(57) Chandler, E. M.; Berglund, C. M.; Lee, J. S.; Polacheck, W. J.; Gleghorn, J. P.; Kirby, B. J.; Fischbach, C. Stiffness of Photocrosslinked RGD-Alginate Gels Regulates Adipose Progenitor Cell Behavior. *Biotechnol. Bioeng.* **2011**, *108* (7), 1683–1692. https://doi.org/10.1002/bit.23079.

(58) Kessler, L.; Gehrke, S.; Winnefeld, M.; Huber, B.; Hoch, E.; Walter, T.; Wyrwa, R.; Schnabelrauch, M.; Schmidt, M.; Kückelhaus, M.; Lehnhardt, M.; Hirsch, T.; Jacobsen, F. Methacrylated Gelatin/Hyaluronan-Based Hydrogels for Soft Tissue Engineering. *J. Tissue Eng.* **2017**, *8*, 2041731417744157. https://doi.org/10.1177/2041731417744157.

(59) Rouillard, A. D.; Berglund, C. M.; Lee, J. Y.; Polacheck, W. J.; Tsui, Y.; Bonassar, L. J.; Kirby, B. J. Methods for Photocrosslinking Alginate Hydrogel Scaffolds with High Cell Viability. *Tissue Eng. Part C Methods* **2010**, *17* (2), 173–179. https://doi.org/10.1089/ten.tec.2009.0582.

(60) Ayer, M. A.; Schrettl, S.; Balog, S.; Simon, Y. C.; Weder, C. Light-Responsive Azo-Containing Organogels. *Soft Matter* **2017**, *13* (22), 4017–4023. https://doi.org/10.1039/C7SM00601B.

(61) Fairbanks, B. D.; Schwartz, M. P.; Bowman, C. N.; Anseth, K. S. Photoinitiated Polymerization of PEG-Diacrylate with Lithium Phenyl-2,4,6-Trimethylbenzoylphosphinate: Polymerization Rate and Cytocompatibility. *Biomaterials* **2009**, *30* (35), 6702–6707. https://doi.org/https://doi.org/10.1016/j.biomaterials.2009.08.055.

(62) Sun, W.; Starly, B.; Daly, A. C.; Burdick, J. A.; Groll, J.; Skeldon, G.; Shu, W.; Sakai, Y.; Shinohara, M.; Nishikawa, M.; Jang, J.; Cho, D.-W.; Nie, M.; Takeuchi, S.; Ostrovidov, S.; Khademhosseini, A.; Kamm, R. D.; Mironov, V.; Moroni, L.; Ozbolat, I. T. The Bioprinting

Roadmap. *Biofabrication* **2020**, *12* (2), 22002. https://doi.org/10.1088/1758-5090/ab5158.

(63) Zhang, J.; Wehrle, E.; Rubert, M.; Müller, R. 3D Bioprinting of Human Tissues: Biofabrication, Bioinks, and Bioreactors. *Int. J. Mol. Sci.* **2021**, *22* (8), 3971.

(64) Rosselin, M.; Xiao, Y.; Belhomme, L.; Lecommandoux, S.; Garanger, E. Expanding the Toolbox of Chemoselective Modifications of Protein-Like Polymers at Methionine Residues. *ACS Macro Lett.* **2019**, *8* (12), 1648–1653. https://doi.org/10.1021/acsmacrolett.9b00862.

(65) Anaya, L. M. B.; Petitdemange, R.; Rosselin, M.; Ibarboure, E.; Garbay, B.; Garanger, E.; Deming, T. J.; Lecommandoux, S. Design of Thermoresponsive Elastin-Like Glycopolypeptides for Selective Lectin Binding and Sorting. *Biomacromolecules* **2021**, *22* (1), 76–85. https://doi.org/10.1021/acs.biomac.0c00374.

(66) El-Mohri, H.; Wu, Y.; Mohanty, S.; Ghosh, G. Impact of Matrix Stiffness on Fibroblast Function. *Mater. Sci. Eng. C* **2017**, *74*, 146–151. https://doi.org/https://doi.org/10.1016/j.msec.2017.02.001.

(67) D Angelo, M.; Benedetti, E.; Tupone, M. G.; Catanesi, M.; Castelli, V.; Antonosante, A.; Cimini, A. The Role of Stiffness in Cell Reprogramming: A Potential Role for Biomaterials in Inducing Tissue Regeneration. *Cells* **2019**, *8*, 1036. https://doi.org/10.3390/cells8091036.

(68) Wang, J.; Wei, Y.; Zhao, S.; Zhou, Y.; He, W.; Zhang, Y.; Deng, W. The Analysis of Viability for Mammalian Cells Treated at Different Temperatures and Its Application in Cell Shipment. *PLoS One* **2017**, *12* (4), e0176120–e0176120. https://doi.org/10.1371/journal.pone.0176120.

(69) Thompson, K. V.; Holliday, R. Effect of Temperature on the Longevity of Human Fibroblasts in Culture. *Exp Cell Res.* **1973**, *80* (2), 354–360. https://doi.org/10.1016/0014-4827(73)90307-8.

(70) Pepper, M. E.; Seshadri, V.; Burg, T. C.; Burg, K. J. L.; Groff, R. E. Characterizing the Effects of Cell Settling on Bioprinter Output. *Biofabrication* **2012**, *4* (1), 11001. https://doi.org/10.1088/1758-5082/4/1/011001.

(71) Schwab, A.; Levato, R.; D'Este, M.; Piluso, S.; Eglin, D.; Malda, J. Printability and Shape Fidelity of Bioinks in 3D Bioprinting. *Chem. Rev.* **2020**, *120* (19), 11028–11055. https://doi.org/10.1021/acs.chemrev.0c00084.

(72) Sivaraman, B.; Bashur, C. A.; Ramamurthi, A. Advances in Biomimetic Regeneration of Elastic Matrix Structures. *Drug Deliv. Transl. Res.* **2012**, *2* (5), 323–350. https://doi.org/10.1007/s13346-012-0070-6.

(73) Coenen, A. M. J.; Bernaerts, K. V; Harings, J. A. W.; Jockenhoevel, S.; Ghazanfari, S. Elastic Materials for Tissue Engineering Applications: Natural, Synthetic, and Hybrid Polymers. *Acta Biomater.* **2018**, *79*, 60–82. https://doi.org/https://doi.org/10.1016/j.actbio.2018.08.027.

(74) Grinnell, F.; Ho, C.-H.; Tamariz, E.; Lee, D. J.; Skuta, G. Dendritic Fibroblasts in Three-Dimensional Collagen Matrices. *Mol. Biol. Cell* **2003**, *14* (2), 384–395. https://doi.org/10.1091/mbc.e02-08-0493.

(75) Niland, S.; Cremer, A.; Fluck, J.; Krieg, T.; Sollberg, S.; Eble, J. A. Contraction-Dependent Apoptosis of Normal Dermal Fibroblasts. *J. Invest. Dermatol.* **2001**, *116* (5), 686–692. https://doi.org/https://doi.org/10.1046/j.1523-1747.2001.01342.x.

(76) Zhang, Z.-G.; Bothe, I.; Hirche, F.; Zweers, M.; Gullberg, D.; Pfitzer, G.; Krieg, T.; Eckes, B.; Aumailley, M. Interactions of Primary Fibroblasts and Keratinocytes with Extracellular Matrix Proteins: Contribution of Alpha2beta1 Integrin. *J. Cell Sci.* **2006**, *119* (9), 1886 LP – 1895. https://doi.org/10.1242/jcs.02921.

(77) Frantz, C.; Stewart, K. M.; Weaver, V. M. The Extracellular Matrix at a Glance. *J. Cell Sci.* **2010**, *123* (24), 4195 LP – 4200. https://doi.org/10.1242/jcs.023820.

(78) Grinnell, F.; Petroll, W. M. Cell Motility and Mechanics in Three-Dimensional Collagen Matrices. *Annu. Rev. Cell Dev. Biol.* **2010**, *26* (1), 335–361. https://doi.org/10.1146/annurev.cellbio.042308.113318.

(79) Ferraris, C. L'ingénieurie Tissulaire "La Peau Reconstruite." *Pour Sci.* **2005**, 8–13.

(80) Ahn, G.; Min, K.-H.; Kim, C.; Lee, J.-S.; Kang, D.; Won, J.-Y.; Cho, D.-W.; Kim, J.-Y.; Jin, S.; Yun, W.-S.; Shim, J.-H. Precise Stacking of Decellularized Extracellular Matrix Based 3D Cell-Laden Constructs by a 3D Cell Printing System Equipped with Heating Modules. *Sci. Rep.* **2017**, *7* (1), 8624. https://doi.org/10.1038/s41598-017-09201-5.

(81) Osidak, E. O.; Karalkin, P. A.; Osidak, M. S.; Parfenov, V. A.; Sivogrivov, D. E.; Pereira, F. D. A. S.; Gryadunova, A. A.; Koudan, E. V; Khesuani, Y. D.; Kasyanov, V. A.; Belousov, S. I.; Krasheninnikov, S. V; Grigoriev, T. E.; Chvalun, S. N.; Bulanova, E. A.; Mironov, V. A.; Domogatsky, S. P. Viscoll Collagen Solution as a Novel Bioink for Direct 3D Bioprinting. *J. Mater. Sci. Mater. Med.* **2019**, *30* (3), 31. https://doi.org/10.1007/s10856-019-6233-y.

(82) DeSimone, E.; Schacht, K.; Pellert, A.; Scheibel, T. Recombinant Spider Silk-Based Bioinks. *Biofabrication* **2017**, *9* (4), 44104. https://doi.org/10.1088/1758-5090/aa90db.

(83) Arai, K.; Tsukamoto, Y.; Yoshida, H.; Sanae, H.; Mir, T. A.; Sakai, S.; Yoshida, T.; Okabe, M.; Nikaido, T.; Taya, M.; Nakamura, M. The Development of Cell-Adhesive Hydrogel for 3D Printing. *Int. J. Bioprinting* **2016**, *2*, 153–162. https://doi.org/10.18063/IJB.2016.02.002.

(84) Rustad, K. C.; Wong, V. W.; Gurtner, G. C. The Role of Focal Adhesion Complexes in Fibroblast Mechanotransduction during Scar Formation. *Differentiation* **2013**, *86* (3), 87–91. https://doi.org/https://doi.org/10.1016/j.diff.2013.02.003.

(85) Tracy, L. E.; Minasian, R. A.; Caterson, E. J. Extracellular Matrix and Dermal Fibroblast Function in the Healing Wound. *Adv. wound care* **2016**, *5* (3), 119–136. https://doi.org/10.1089/wound.2014.0561.

(86) Mewes, K. R.; Raus, M.; Bernd, A.; Zöller, N. N.; Sättler, A.; Graf, R. Elastin Expression in a Newly Developed Full-Thickness Skin Equivalent. *Skin Pharmacol. Physiol.* **2007**, *20* (2), 85–95. https://doi.org/10.1159/000097655.

(87) Kim, B. S.; Kwon, Y. W.; Kong, J.-S.; Park, G. T.; Gao, G.; Han, W.; Kim, M.-B.; Lee, H.; Kim, J. H.; Cho, D.-W. 3D Cell Printing of in Vitro Stabilized Skin Model and in Vivo Pre-Vascularized Skin Patch Using Tissue-Specific Extracellular Matrix Bioink: A Step towards Advanced Skin Tissue Engineering. *Biomaterials* **2018**, *168*, 38–53. https://doi.org/https://doi.org/10.1016/j.biomaterials.2018.03.040.

(88) Rimann, M.; Bono, E.; Annaheim, H.; Bleisch, M.; Graf-Hausner, U. Standardized 3D Bioprinting of Soft Tissue Models with Human Primary Cells. *J. Lab. Autom.* **2015**, *21* (4), 496–509. https://doi.org/10.1177/2211068214567146.

(89) Debret, R.; Faye, C.; Sohier, J.; Sommer, P. Polypeptide Dérivé de La Tropoélastine et Matériau Biocompatible Le Comprenant (WO 2017/194761 A2), 2017.

(90) Shi, Y.; Xing, T. L.; Zhang, H. B.; Yin, R. X.; Yang, S. M.; Wei, J.; Zhang, W. J. Tyrosinase-Doped Bioink for 3D Bioprinting of Living Skin Constructs. *Biomed. Mater.* **2018**, *13* (3), 35008. https://doi.org/10.1088/1748-605x/aaa5b6.

(91) Baltazar, T.; Merola, J.; Catarino, C.; Xie, C. B.; Kirkiles-Smith, N. C.; Lee, V.; Hotta, S.; Dai, G.; Xu, X.; Ferreira, F. C.; Saltzman, W. M.; Pober, J. S.; Karande, P. Three Dimensional Bioprinting of a Vascularized and Perfusable Skin Graft Using Human Keratinocytes, Fibroblasts, Pericytes, and Endothelial Cells. *Tissue Eng. Part A* **2019**, *26* (5–6), 227–238. https://doi.org/10.1089/ten.tea.2019.0201.

(92) Cubo, N.; Garcia, M.; del Cañizo, J. F.; Velasco, D.; Jorcano, J. L. 3D Bioprinting of Functional Human Skin: Production and in Vivo Analysis. *Biofabrication* **2016**, *9* (1), 15006. https://doi.org/10.1088/1758-5090/9/1/015006.

(93) Cheng, L.; Yao, B.; Hu, T.; Cui, X.; Shu, X.; Tang, S.; Wang, R.; Wang, Y.; Liu, Y.; Song, W.; Fu, X.; Li, H.; Huang, S. Properties of an Alginate-Gelatin-Based Bioink and Its Potential Impact on Cell Migration, Proliferation, and Differentiation. *Int. J. Biol. Macromol.* **2019**, *135*, 1107–1113. https://doi.org/https://doi.org/10.1016/j.ijbiomac.2019.06.017.

(94) Jorgensen, A. M.; Varkey, M.; Gorkun, A.; Clouse, C.; Xu, L.; Chou, Z.; Murphy, S. V; Molnar, J.; Lee, S. J.; Yoo, J. J.; Soker, S.; Atala, A. Bioprinted Skin Recapitulates Normal Collagen Remodeling in Full-Thickness Wounds. *Tissue Eng. Part A* **2019**, *26* (9–10), 512–526. https://doi.org/10.1089/ten.tea.2019.0319.

(95) Zidarič, T.; Milojević, M.; Gradišnik, L.; Stana Kleinschek, K.; Maver, U.; Maver, T. Polysaccharide-Based Bioink Formulation for 3D Bioprinting of an In Vitro Model of the Human Dermis. *Nanomater. (Basel, Switzerland)* **2020**, *10* (4), 733. https://doi.org/10.3390/nano10040733.

Author manuscript of article published in *Biomacromolecules*, DOI: 10.1021/acs.biomac.1c00861

Supporting Information for:

Elastin-like polypeptide based bioink: a promising alternative for 3D bioprinting

Michèle Dai, [†,‡] *Jean-Philippe Belaïdi,* [†] *Guillaume Fleury,* [‡] *Elisabeth Garanger,* [‡] *Maïté Rielland,* [*,†] *Xavier Schultze,* [†] *Sébastien Lecommandoux*[‡]

[†] L'Oréal Recherche Avancée, 1 avenue Eugène Schueller, 93600, Aulnay-sous-Bois, France

[‡] Univ. Bordeaux, CNRS, Bordeaux INP, LCPO, UMR 5629, F-33600, Pessac, France

a/ Reagents

Acetic acid, lithium phenyl-2,4,6-trimethylbenzoylphosphinate (LAP), *N*-hexylamine and poly(ε-caprolactone) (PCL) (Mn 45,000 #704105) were purchased from Sigma-Aldrich (France). Glycidyl acrylate and 1,1,1,3,3,3-hexafluoro-2-propanol (HFIP) were obtained from TCI Chemicals (Belgium). Mercaptopropionic acid-(Gly-Arg-Gly-Asp-Ser)-OH (MPA-GRGDS-OH) was purchased from Provepharm (France). Ultrapure water (18 MΩ·cm) was obtained by passing in-house deionized water through a Millipore Milli-Q Biocel A10 purification unit. DMEM (1X) + GlutaMAX (Dulbecco's Modified Eagle *Medium* (DMEM) [+] 4.5 g/L D-glucose, [+] pyruvate, Ref. 31966-021), Anti-Anti (100X) (Antibiotic-Antimycotic containing 10,000 units/mL of penicillin, 10,000 µg/mL of streptomycin, and 25 µg/mL of Gibco amphotericin B, Ref. 15240-062) and Dulbecco phosphate buffer saline (DPBS), a saline buffer solution without calcium and magnesium, were purchased from Gibco® (France). Bovine calf serum supplemented HyClone® (Fe^{2+} supplemented fetal bovine serum (FBS), Hyclone AXB30110) and live/dead test kit were acquired from Thermo Scientific (France). Type I acido soluble Collagen from calf hides (5 mg/ml with 0.017 N acetic acid) were ordered from Symatese (France). Cellulose nanofibers (CNF) at 6 wt% in DPBS were purchased from VTT (Finland). CellTiter-Glo® 3D, cell viability assay kit was obtained from Promega (France). Green 7F (G7F) and green 3F (G3F) was purchased from EPISKIN (France).

	Primary antibody	**Secondary antibody**
Vimentin	abcam, ab6328 (1/100)	A21422, Mouse (1/500)
Pro collagen I	Millipore, MAB1912 (1/100)	A21434, Rat (1/500)
Collagen I	Millipore, MAB3391 (1/200)	A21422, Mouse (1/500)
Elastin	Novotec, 25011 (1/200)	A21428, Rabbit (1/500)
Fibrillin	Millipore, MAB1919 (1/400)	A21422, Mouse (1/500)
Fibronectin	abcam, ab6328 (1/100)	A21422, Mouse (1/500)

Table S1. Primary and secondary antibodies associated to specific markers.

b/ Characterization techniques

i. Sodium dodecyl sulfate-polyacrylamide gel electrophoresis (SDS-PAGE)

ELPs were separated under reducing conditions by SDS-PAGE with 4-15 % Mini-PROTEIN® TGX precast protein gel (Bio-Rad) and Tris/Glycine/SDS buffer (Bio-Rad). Polypeptide bands were detected by the stain-free technique with Bio-Rad Gel Doc EZ system.

ii. Matrix-assisted laser desorption/ionization (MALDI)

Mass spectrometry analysis was performed on a MALDI-ToF-ToF (time of flight) (Ultraflex III, Bruker) equipped with a matrix-assisted laser desorption/ionization source. ELP samples were prepared as following: freeze-dried compounds were dissolved in cold water (2 mg/mL) and were then mixed to the matrix solution: sinapinic acid (10 mg/mL in acetonitrile/0.1% trifluoroacetic acid in water (1/1, v/v)). Then, a 1-2 µL of this solution were added to a metal plate. After solvent evaporation, the solid residue was exposed under laser (Smartbeam, Nd:YAG, 355 nm). Analysis were performed in positive linear mode, and proteins standards mixture were used for external calibration of the instrument in a mass range adapted to proteins of interest.

iii. Nuclear magnetic resonance (NMR)

NMR *spectra* of ELP-containing samples in D_2O were acquired at 298 K on an AVANCE III HD 400 spectrometer operating at 400.2 MHz for ^1H. The solvent signal was used as the reference signal. *Data* processing was performed using Topspin software.

iv. Dynamic light scattering (DLS) for transition temperature measurement

For ELPs transition temperatures determination, DLS were performed on a NanoZS instrument (Malvern, U.K.) at a 178° angle and at a constant position in the cuvette. Solutions of *MW*-ELP[V_3M_1-40] and derivatives were prepared at 750 µM in UP water. Temperature was raised from 15 to 70°C. Three independent measurements of eleven 10 seconds, were recorded and averaged at every 2°C after a 1 min-temperature equilibration time. The scattering light intensities were normalized and plotted as a function of temperature.

c/ Development and characterization of MW-ELP[V_3M_1-40]

An elastin-like polypeptide (ELP) with the primary structure *MW*[VPGVGVPGMG(VPGVG)$_2$]$_{10}$ was designed and produced using recombinant DNA and protein engineering techniques.

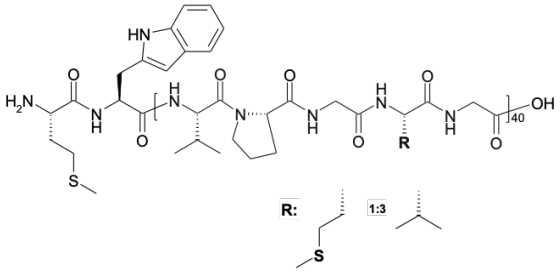

Figure S1. *MW*-ELP[V_3M_1-40] Elastin-like polypeptide representation.

The *MW*-ELP[V_3M_1-40]-encoding gene was obtained by recursive directional ligation of a commercially sourced *MW*-ELP[V_3M_1-20] [46]. A clone expressing the ELP was cultured in *E. coli* for 21 hours after induction by isopropyl-β-D-thiogalactoside (IPTG). Soluble proteins were extracted from the cell lysate. The ELP was then purified by inverse transition cycling (ITC), dialyzed extensively against ultrapure water (UP) and lyophilized to provide pure protein in 150 mg/L culture yields. The purity of the ELP was assessed by SDS-PAGE (Figure S2). MALDI mass

spectrometry were performed to determine an experimental mass of 17,040 Da in agreement with the theoretical value (Figure S3). The protein was characterized by ^{1}H NMR spectroscopy, confirming the ELP structure (Figure S4).

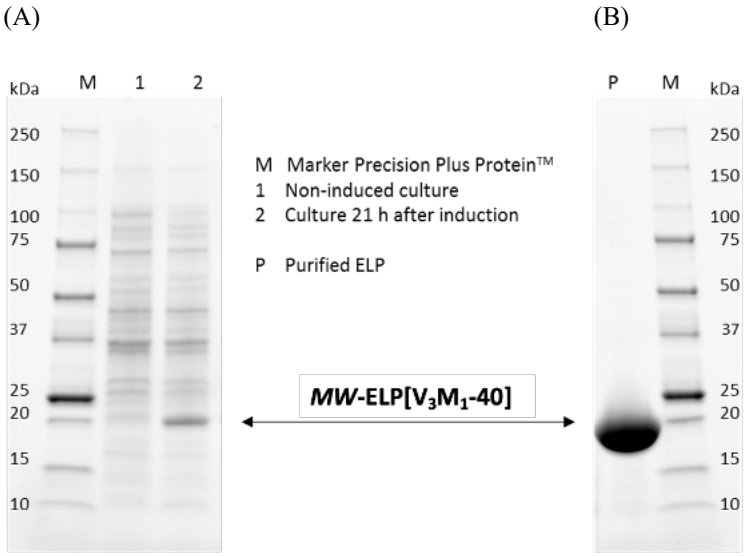

Figure S2. (A) Expression of recombinant *MW*-ELP[V_3M_1-40] during bacterial fermentation and **(B)** purified ELP, as analyzed by SDS-PAGE.

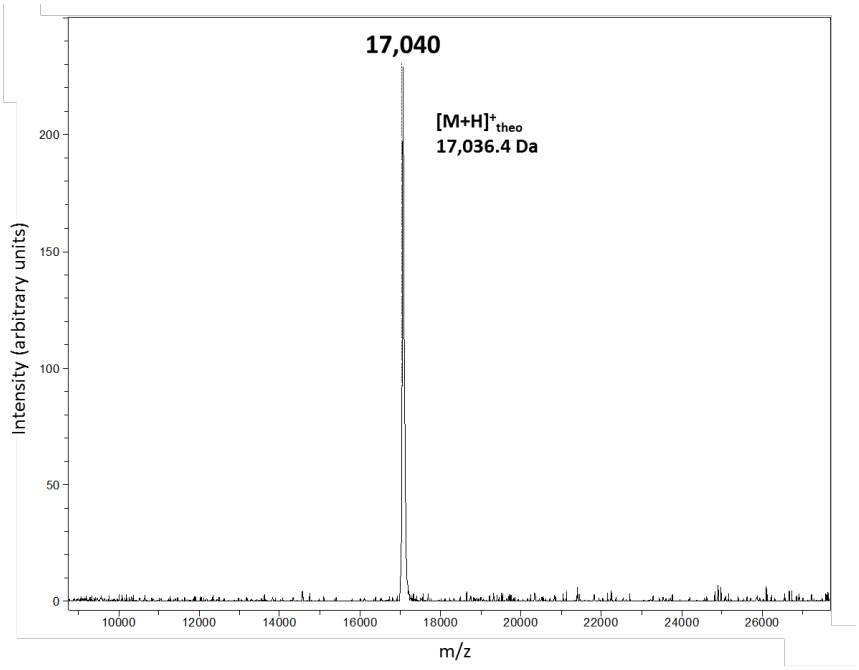

Figure S3. MALDI mass *spectra* of *MW*-ELP[V_3M_1-40]. $[M+H]^{+}_{theo}$ = theoretical mass.

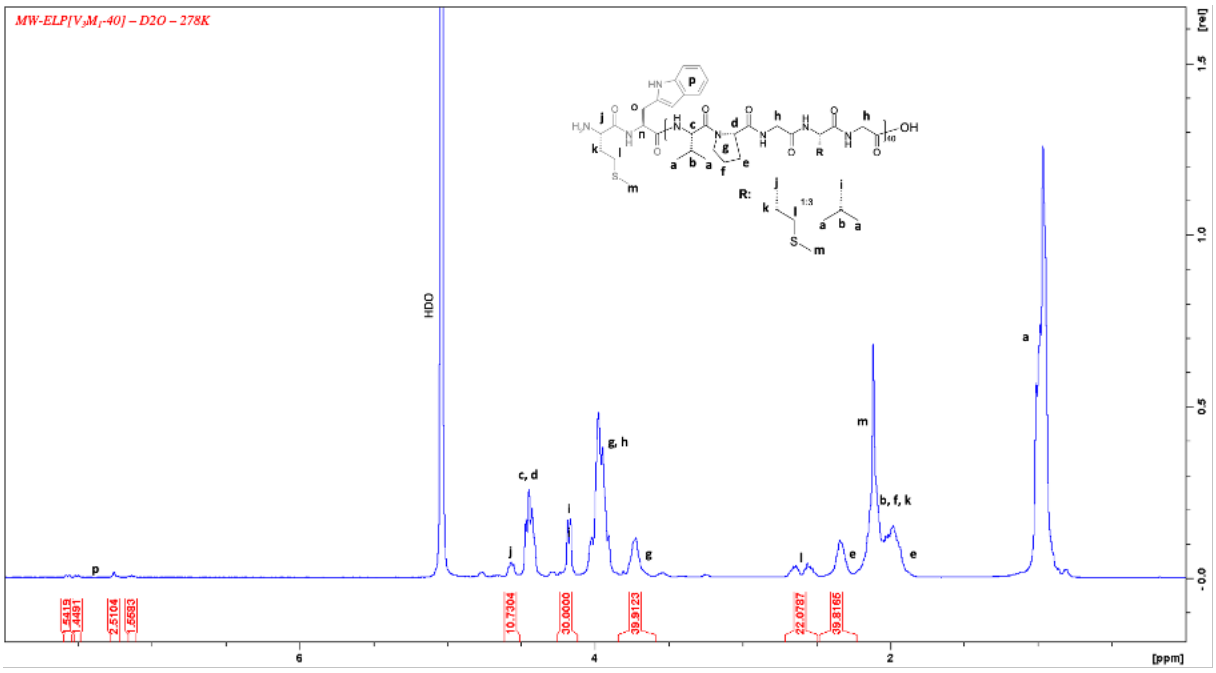

Figure S4. *MW*-ELP[V_3M_1-40] ^{1}H NMR *spectrum* in D_2O at 278K.

d/ Characterization of modified MW-ELP[V_3M_1-40] with acrylates

The degree of functionalization of modified ELP with acrylates, was assessed by performing ^{1}H NMR (Figure S5). Two ways to determine this value have been used: firstly, by using the integration at δ = 3.0 ppm corresponding to the three protons of –SC*H*$_3$ methionine residues (noted *m* in the *spectra*) and secondly, by integrating the different peaks at δ = 6.0, 6.3 and 6.5 ppm (noted *s*, *q*, *r*, respectively) corresponding each to protons on acrylate double bounds. These integrations were calibrated by assigning the resonances at δ = 4.5 ppm (noted *c*, *d*) to the protons of the valine and proline side chains. Thus, excellent degrees of functionalization were obtained for the synthesized compound, estimated at > 99 %. The slight decrease in degrees of alkylation were due to a small amount of methionine oxidation into sulfoxide during the reaction evidenced by the existence of resonance at δ = 2.7 ppm in the ^{1}H NMR *spectrum* corresponding to –S(O)C*H*$_3$. A single peak integrating for 32.8 protons is noticeable on the *spectrum* at δ = 1.9 ppm, which

corresponds to the CH_3 of CH_3COO^-, counterion of the sulfonium as the reaction was perfomed in acidic condition.

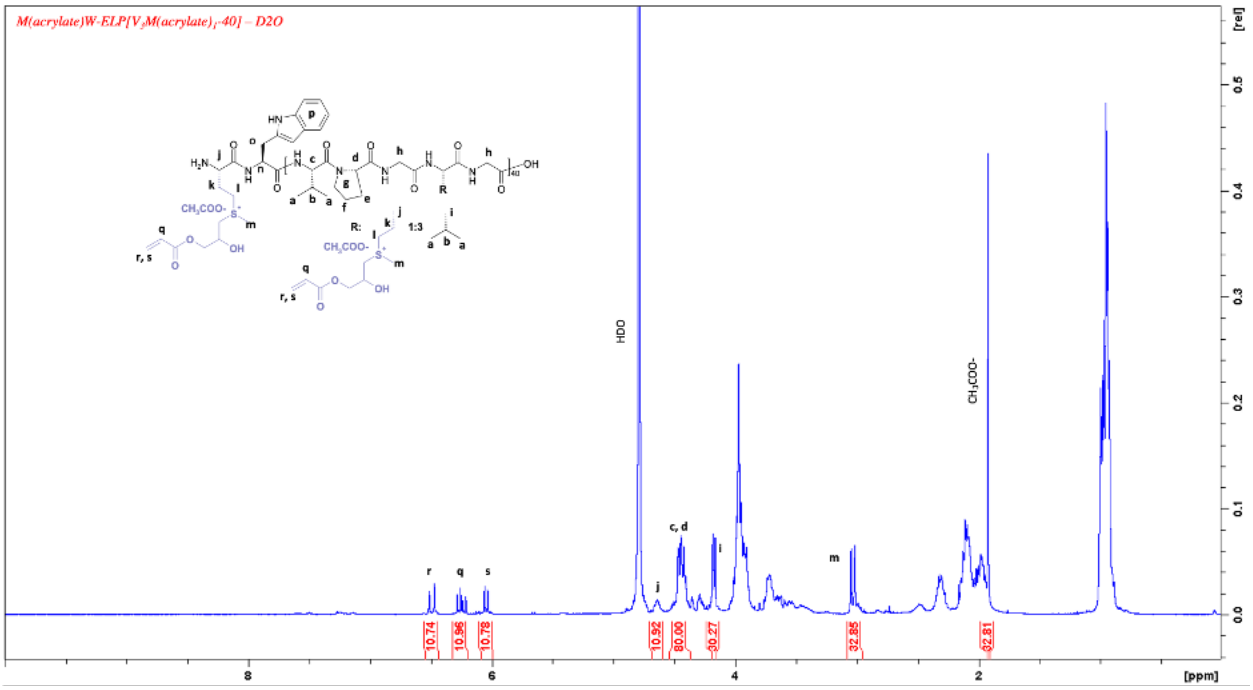

Figure S5. ^{1}H NMR *spectrum* of modified *MW*-ELP[V_3M_1-40]: *M*(acrylate)*W*-ELP[V_3M(acrylate)$_1$-40].

e/ Characterization of modified MW-ELP[V_3M_1-40] with GRGDS

To identify peaks associated to protons of modified ELPs with GRGRDS moieties, the ^{1}H NMR *spectrum* of MPA-GRGDS-OH has been performed (Figure S6A), revealing the two protons CH_2-NH-C(NH)-NH_2 (noted *G*) and those from CH_2-CH_2-NH-C(NH)-NH_2 (noted *L*) of arginine at δ = 3.25 ppm and 1.68 ppm, respectively. To determine the degree of functionalization, the resonance at δ = 4.5 ppm corresponding to the αCH protons of the valine and proline (noted *c*, *d*) was considered as standard. After modification, for 30 %-targetted GRGDS functionalization, the integrations of acrylate protons decreased from 11 to 7.7 meaning that 30 % of acrylates have been modified (Figure S6B). Moreover, the two protons CH_2-NH-C(NH)-NH_2 (noted *G*) and those from CH_2-CH_2-NH-C(NH)-NH_2 (noted *L*) of arginine at δ = 3.25 ppm and 1.68 ppm, respectively

appeared on the *spectrum* and integrated for 6.7 protons meaning that 3.35 GRGDS moieties have been grafted, which is consistent with the 30 % modified acrylates.

(A)

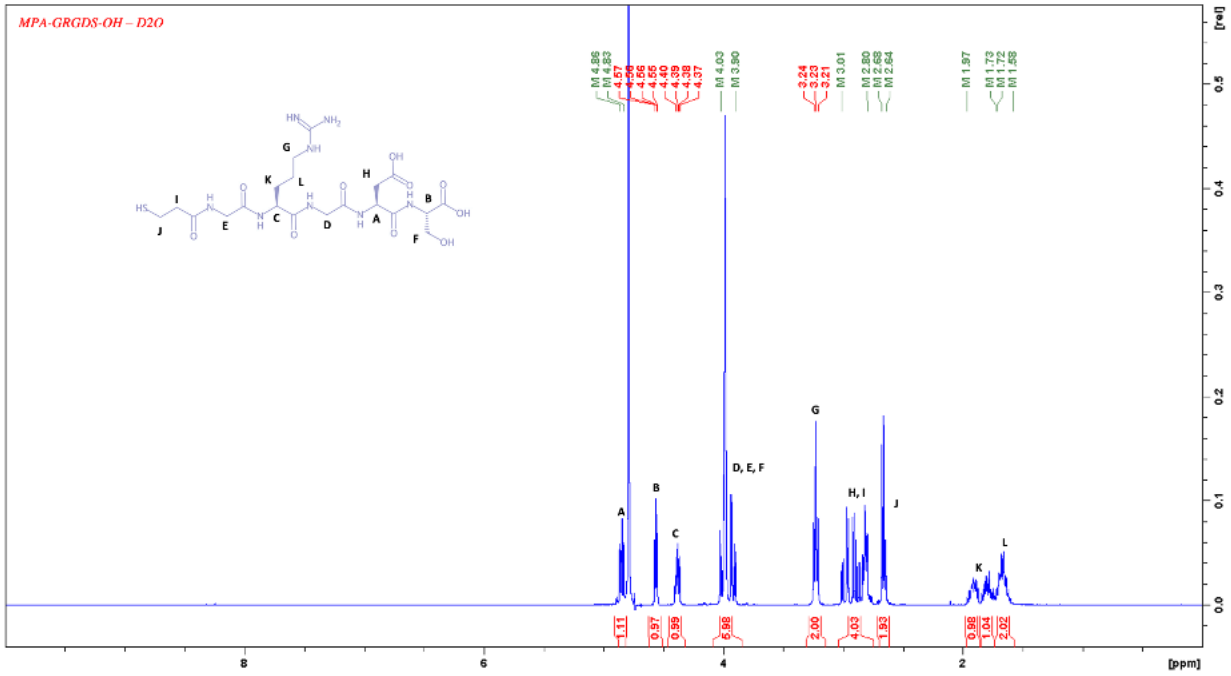

(B)

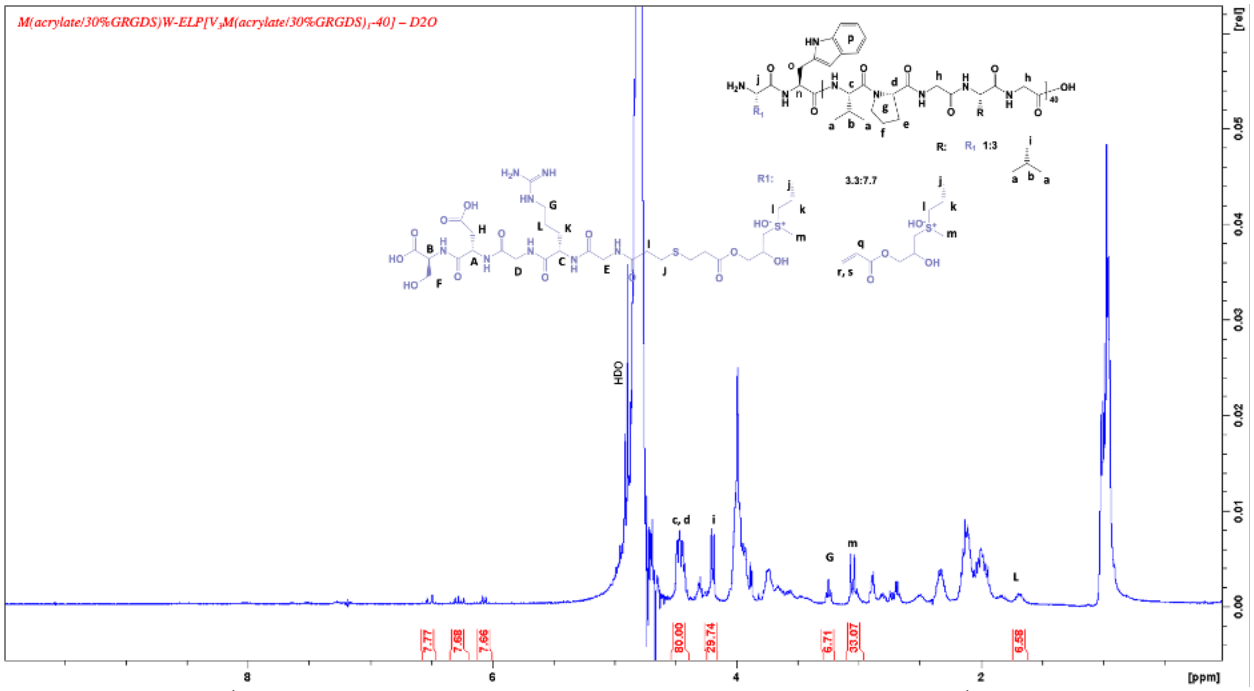

Figure S6. (A) ^{1}H NMR *spectrum* of MPA-GRGDS-OH in D_2O. **(B)** ^{1}H NMR *spectrum* of *M*(acrylate/30%GRGDS)*W*-ELP[V_3M(acrylate/30%GRGDS)$_1$-40] in D_2O.

f/ Loss of thermosensitivity through post-modification of ELP

Dynamic light intensity (DLS) measurements have been performed to conclude on the loss of thermosensitivity for chemically modified *MW*-ELP[V_3M_1-40] in UP water after chemical modification reactions (Figure S7). Moreover, the transition temperature (T_t) is dependent on the concentration of the solution: the higher the concentration, the lower the T_t [51]. Thus, measurements at relatively high concentration (750 µM) were performed to be able to differentiate the modified ELPs thermal behaviors.

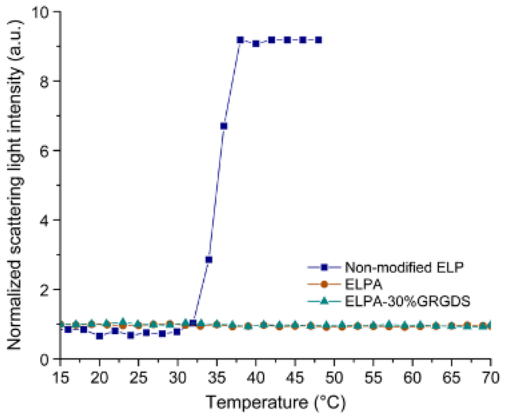

Figure S7. Evolution of the scattering light intensity of non-modified ELP, ELPA and ELPA-30%GRGDS solutions at 750 µM in UP water, as a function of temperature at a 173° scattering angle.

The non-modified ELP has a transition temperature associated to a change in structural behaviour, classical for an ELP monoblock [51]. The totally soluble ELP chain at low temperature turns to form micro-size coacervates at high temperature. In the case of ELPA at 750 µM, the introduction of acrylates on ELP methionines eliminates the transition temperature as no change in intensity appears along the increase of temperature. The grafting of acrylates creates a sulfonium, which is charged; it can increase the hydrophilicity of the ELP chain. As reported, the higher the hydrophilicity of the ELP, the higher its T_t would be [50]. Thus, if too hydrophilic, no T_t appears anymore. However, sulfoniums may have modified the properties of ELP, eliminating the

coacervation event. The same experiments were performed for ELPA-30%GRGDS at 750 µM. Similarly, as expected, no transition temperature was visible for each modified ELPs. Indeed, GRGDS is a hydrophilic peptide, making ELPA-30%GRGDS even more hydrophilic.

g/ Evaluation of LAP toxicity and phototoxicity

The tests consist in a luminescence cell viability assay for each condition. In more details, the cell viability assay involves using a kit called Cell-Titer Glo® which determines the number of viable cells in culture based on the quantification of the present adenosine triphosphate (ATP), an indicator of cell metabolic activity. Briefly, one milliliter containing 15,000 dermal normal human fibroblast cells in FM were plated in 24-wells plates and kept in a humidified culture incubator at 37°C and with 5 % CO_2 for 48 hours. Then, 12 concentrations of LAP were considered and prepared by serial dilution in FM (2*0.3 % w/v, 0.1 % w/v, 0.05 % w/v, 0.025 % w/v, 0.01 % w/v, 0.005 % w/v, 0.0025 % w/v, 0.001 % w/v, 0.0005 % w/v ,2*NT (non-treated)), with four repetitions. FM was removed from each well and 400 µl of each concentration were added. They were incubated in a humified atmosphere at 37°C and with 5 % CO_2 for 30 minutes. All wells except one condition of 0.3 % w/v and one NT, were exposed under UV-light for 2 min 24 s, under UV 365 nm with 7.91 mW/cm² of a solar simulator (SOL-UV-6 equipped with 2 filters: WG360 and UG11) (corresponding to 15 s under a UV source at 365 nm with 76.2 mW/cm²). *Media* were all removed from wells and 1 mL of FM were added. Plates were kept for 24 hours in a humidified culture incubator at 37°C and with 5 % CO_2. Then, for each condition, *medium* was removed and they were then treated with CellTiter Glo kit to determine cells viability. Briefly, after 30 minutes of contact with the reagents provided by the kit, and transferred to a 96-well white plate (Corning), luminescent signals, more precisely relative light units (RLU) were measured with a GloMax® Discover Microplate Reader (Figure S8).

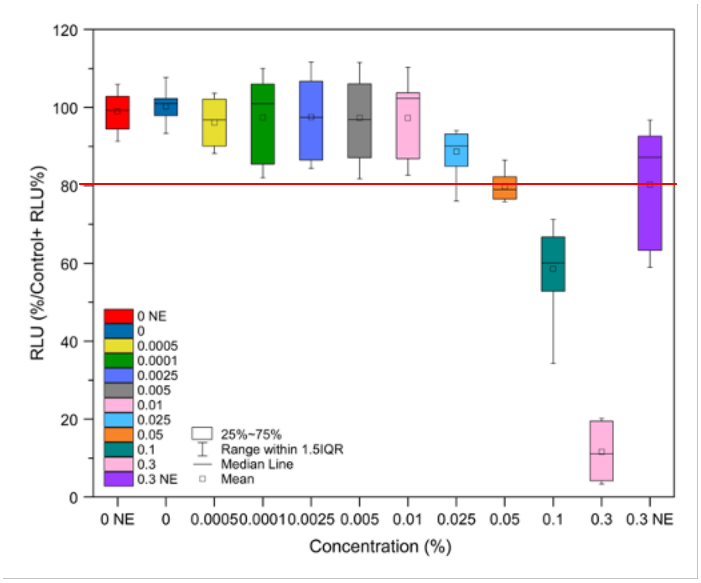

Figure S8. *Ratio* of relative light units (RLU) over control+'s RLU *via* Cell-Titer Glo® luminescent cell viability assay of 2D-cultured human fibroblasts in FM, exposed under UV-light at 365 nm in contact with LAP (from 0 to 0.3 wt%) after 24 hours, except those quoted with NE (non-exposed). Red line = 80 % viability limit.

h/ Bioink elasticity

i. Macroscopic elasticity

As shown in Figure S9 and Video S1, when a stress is applied to a cross-linked bioink sample (Figure S9(1-2)), and is then removed (Figure S9(3-6)), a complete recovery of its shape is retrieved.

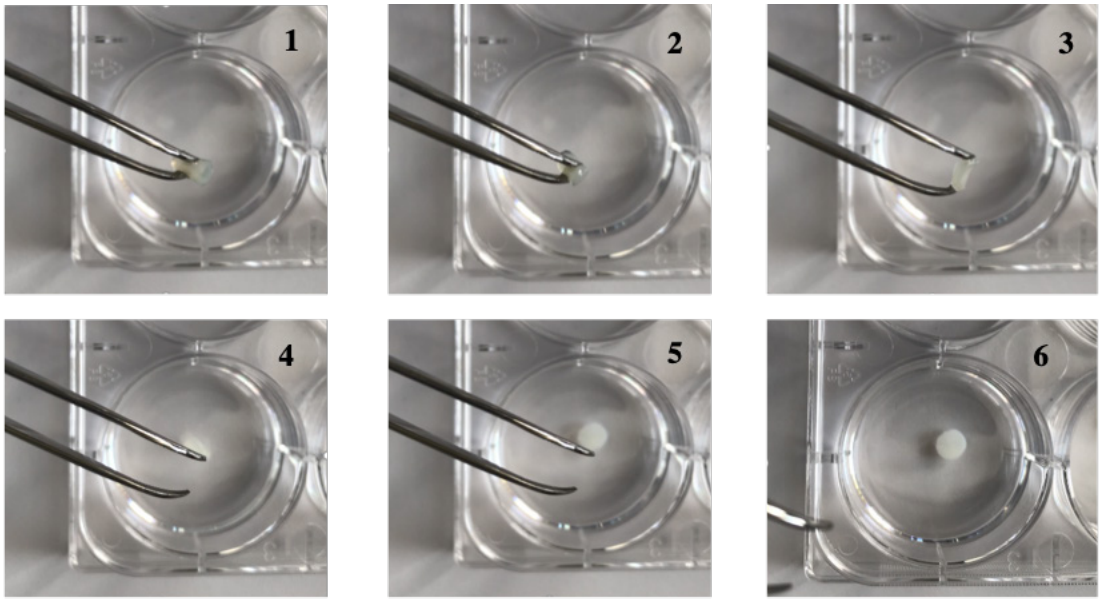

Figure S9. Shape evolution of cross-linked bioink under manual stress.

Video S1. Shape evolution of cross-linked bioink under manual stress.

ii. Strain recovery after creep test

The strain recovery behavior of the cross-linked bioinks was evaluated using an approach based on Kohlrausch-Williams-Watts / Weibull distribution function to describe the relaxation process. (10.1007/s10853-005-2020-x)

In this approach, the time-dependent recovery strain, $\varepsilon_{recovery}$, following the instantaneous strain recovery, is expressed using a "stretched exponential" function as:

$$\varepsilon_{recovery}(t) = \varepsilon_{visc}(t)\left[exp\left(-\left(\frac{t}{t_r}\right)^{\beta}\right)\right] + \varepsilon_{irr} \quad \textbf{(1)}$$

Where ε_{visc} is the viscoelastic strain recovery, t_r the characteristic relaxation time, β the shape exponent of the stretched exponential decay and ε_{irr} the irreversible strain from viscous flow.

Figure S10 shows the time-dependent recovery strain of the cross-linked bioinks as a function of the initial stress loading. The parameters obtained from fitting time-dependent recovery strain curves to experimental data are summarized in Table S2.

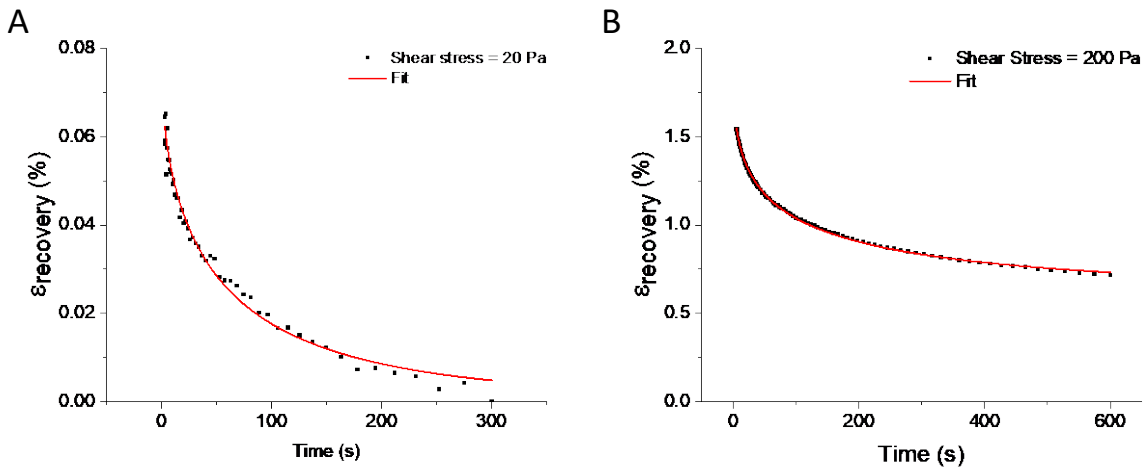

Fig S10. Time-dependent recovery strain of the cross-linked bioinks as a function of the initial stress loading. **A** – for an initial shear stress of 20 Pa and **B** – for an initial shear stress of 200. The red continuous lines are best fitting curves using equation **(1)**.

Table S2. Parameters obtained from fitting time-dependent recovery strain curves to experimental data using equation **(1)**.

τ_0 (Pa)[a]	ε_{visc} (%)[b]	t_r (s)[c]	β[d]	ε_{irr} (%)[f]	Reduced χ^2
20	0.075 ± 0.003	53.33 ± 4.91	0.58 ± 0.04	0	$6.1\ 10^{-6}$
200	1.33 ± 0.02	76.65 ± 2.20	0.41 ± 0.01	0.6	$4.7\ 10^{-5}$

[a] τ_0, initial shear stress. [b] ε_{visc}, viscoelastic strain recovery. t_r, characteristic relaxation time. β, Shape exponent of the stretched exponential decay ($\beta = 1$ refers to a single relaxation time and $\beta < 1$ indicates a broader distribution of relaxation times). ε_{irr}, permanent strain from viscous flow (ε_{irr} was fixed to a asymptotic value of $\varepsilon_{irr}(\tau_0 = 20\ Pa) = 0\%$ and $\varepsilon_{irr}(\tau_0 = 200\ Pa) = 0.6\%$ during the fitting process).

i/ Printing fidelity

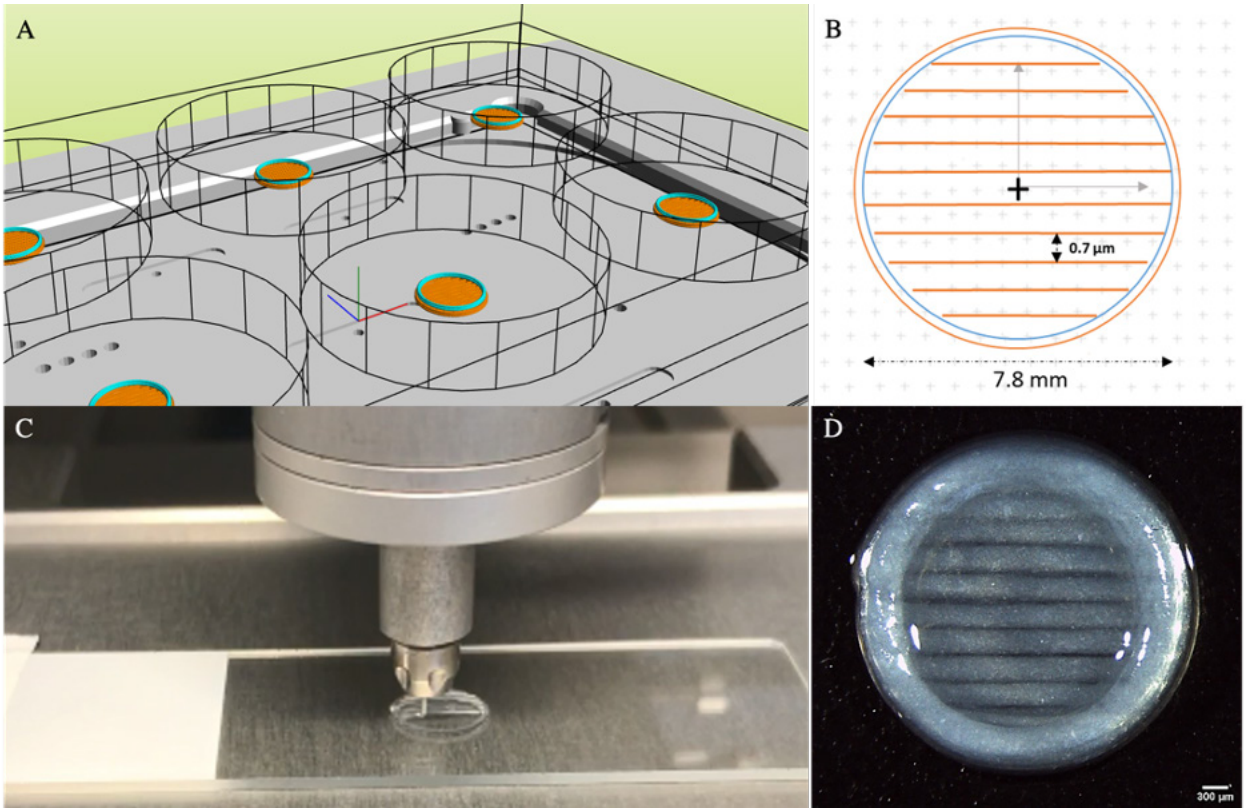

Figure S11. **(A)** Numerical 2D design drawn on regen Hu's BioCAD. **(B)** Numerical 3D design visualization. **(C)** View of inkjet bioprinting process. **(D)** Picture taken with a stereo microscope Leica M60 with an integrated Leica IC80 high-definition camera, scale bar: 300 μm.

Video S2. Inkjet bioprinting process in real time.